

3 | Spotlight Selection | Applied and Industrial Microbiology | Full-Length Text

# Overexpression of RuBisCO form I and II genes in *Rhodopseudomonas palustris* TIE-1 augments polyhydroxyalkanoate production heterotrophically and autotrophically

Tahina Onina Ranaivoarisoa,<sup>1</sup> Wei Bai,<sup>2</sup> Rengasamy Karthikeyan,<sup>1</sup> Hope Steele,<sup>1</sup> Miriam Silberman,<sup>1</sup> Jennifer Olabode,<sup>1</sup> Eric Conners,<sup>1</sup> Brian Gallagher,<sup>1</sup> Arpita Bose<sup>1</sup>

**AUTHOR AFFILIATIONS** See affiliation list on p. 23.

ABSTRACT With the rising demand for sustainable renewable resources, microorganisms capable of producing bioproducts such as bioplastics are attractive. While many bioproduction systems are well-studied in model organisms, investigating non-model organisms is essential to expand the field and utilize metabolically versatile strains. This investigation centers on Rhodopseudomonas palustris TIE-1, a purple non-sulfur bacterium capable of producing bioplastics. To increase bioplastic production, genes encoding the putative regulatory protein PhaR and the depolymerase PhaZ of the polyhydroxyalkanoate (PHA) biosynthesis pathway were deleted. Genes associated with pathways that might compete with PHA production, specifically those linked to glycogen production and nitrogen fixation, were deleted. Additionally, RuBisCO form I and II genes were integrated into TIE-1's genome by a phage integration system, developed in this study. Our results show that deletion of phaR increases PHA production when TIE-1 is grown photoheterotrophically with butyrate and ammonium chloride (NH<sub>4</sub>CI). Mutants unable to produce glycogen or fix nitrogen show increased PHA production under photoautotrophic growth with hydrogen and NH<sub>4</sub>Cl. The most significant increase in PHA production was observed when RuBisCO form I and form I & II genes were overexpressed, five times under photoheterotrophy with butyrate, two times with hydrogen and  $NH_4CI$ , and two times under photoelectrotrophic growth with  $N_2$ . In summary, inserting copies of RuBisCO genes into the TIE-1 genome is a more effective strategy than deleting competing pathways to increase PHA production in TIE-1. The successful use of the phage integration system opens numerous opportunities for synthetic biology in TIE-1.

**IMPORTANCE** Our planet has been burdened by pollution resulting from the extensive use of petroleum-derived plastics for the last few decades. Since the discovery of biodegradable plastic alternatives, concerted efforts have been made to enhance their bioproduction. The versatile microorganism *Rhodopseudomonas palustris* TIE-1 (TIE-1) stands out as a promising candidate for bioplastic synthesis, owing to its ability to use multiple electron sources, fix the greenhouse gas CO<sub>2</sub>, and use light as an energy source. Two categories of strains were meticulously designed from the TIE-1 wild-type to augment the production of polyhydroxyalkanoate (PHA), one such bioplastic produced. The first group includes mutants carrying a deletion of the *phaR* or *phaZ* genes in the PHA pathway, and those lacking potential competitive carbon and energy sinks to the PHA pathway (namely, glycogen biosynthesis and nitrogen fixation). The second group comprises TIE-1 strains that overexpress RuBisCO form I or form I & II genes inserted via a phage integration system. By studying numerous metabolic mutants and

**Editor** Gemma Reguera, Michigan State University, East Lansing, Michigan, USA

Address correspondence to Arpita Bose, abose@wustl.edu.

Tahina Onina Ranaivoarisoa and Wei Bai contributed equally to this article. Author order was determined at random.

The authors declare no conflict of interest.

See the funding table on p. 23.

Received 18 July 2024 Accepted 30 July 2024 Published 20 August 2024

Copyright © 2024 Ranaivoarisoa et al. This is an open-access article distributed under the terms of the Creative Commons Attribution 4.0 International license

Downloaded from https://journals.asm.org/journal/aem on 01 July 2025 by 75.133.168.157.

overexpression strains, we conclude that genetic modifications in the environmental microbe TIE-1 can improve PHA production. When combined with other approaches (such as reactor design, use of microbial consortia, and different feedstocks), genetic and metabolic manipulations of purple nonsulfur bacteria like TIE-1 are essential for replacing petroleum-derived plastics with biodegradable plastics like PHA.

**KEYWORDS** *Rhodopseudomonas palustris* TIE-1, bioplastics, polyhydroxyalkanoate, *phaR*, *phaZ*, glycogen, *nifA*, RuBisCO

Recent improvements in genetic engineering tools have enabled scientists to systematically engineer organisms that produce various value-added chemicals, including biofuels, therapeutic products, food, and bioplastics (1-3). At first, most of these engineering efforts were focused on widely used model organisms, such as Escherichia coli, Saccharomyces cerevisiae, and Synechococcus sp. MIT9509 (4-8). This emphasis resulted in an array of genetic tools that have been effectively developed for valuable biomolecule biosynthesis and for conducting physiological studies (8-22). However, the reliance on organic carbon as the primary carbon source poses a limitation for heterotrophic model organisms, contributing to elevated bioproduction costs (15-17). Recent studies have highlighted numerous advantages in utilizing non-model organisms for bioproduction (23-25). Over the past decade, one such group of microbes that has gained attention is the purple nonsulfur bacteria exemplified by Rhodopseudomonas palustris TIE-1 (TIE-1) (26–28), Rhodospirillum rubrum (29, 30) and Rhodomicrobium (21, 31). TIE-1, a Gram-negative purple nonsulfur photosynthetic bacterium is renowned for its versatile metabolism, rendering it an excellent host for diverse bioproduction and pathway studies (26, 27). TIE-1 exhibits four primary metabolisms: chemoautotrophy, photoautotrophy, chemoheterotrophy, and photoheterotrophy (26, 27). These different metabolisms enable TIE-1 to use a wide variety of carbon sources such as carbon dioxide (CO<sub>2</sub>) and many organic acids. TIE-1 can use ammonium salts such as ammonium chloride (NH<sub>4</sub>Cl) or fix nitrogen from dinitrogen gas (N<sub>2</sub>) as a nitrogen source (26). Moreover, it can use multiple electron sources including hydrogen (H<sub>2</sub>) or ferrous iron (Fe (II)). One of the most appealing features of TIE-1 is its ability to acquire electrons directly from a poised electrode, which enables us to use it in microbial electrosynthesis (MES) (27, 32–35). MES is a system in which microorganisms are used to produce valuable compounds using their ability to obtain electrons from the bioelectrical reactor (33, 35, 36). Using electrons from a poised electrode or a solar panel-powered MES system, TIE-1 produces biodegradable plastic and biofuel using CO2 as a carbon source, N2 as a nitrogen source, and light as an energy source (27, 37). These represented the first steps toward a sustainable and carbon-neutral process for bioproduction using TIE-1 in MES. Besides its ability to utilize various substrates, TIE-1's metabolic diversity also makes it an extraordinary model organism for pathway investigation (38, 39). For example, the use of RuBisCO mutants allowed us to study the association between the Calvin-Benson-Bassham (CBB) cycle in carbon fixation and extracellular electron transport (40). Similarly, a TIE-1 ΔpioABC mutant was used to investigate the electron uptake mechanism during photoferrotrophic and electrotrophic growth conditions (38). During these studies, mutants were first generated and grown under heterotrophic growth conditions in which the electron uptake machineries were not involved. These strains were then switched to autotrophic and electron uptake growth conditions to further understand their role in metabolism (38, 40). Not only do these studies provide insights into TIE-1's metabolism, but they also open doors for a deeper understanding of other closely related purple nonsulfur bacteria, such as Rhodopseudomonas palustris CGA009, which has been studied extensively for biohydrogen production (41, 42).

The available genetic tools for TIE-1 are limited compared to widely used model organisms, with most tools being based on homologous recombination (34, 40). Fig. S1 illustrates the two-step homologous recombination process for achieving gene integration in TIE-1. Although this process results in markerless strains, it is

time-consuming, with an efficiency lower than 50% (34). To reduce processing time and enhance efficiency, we explored phage recombination techniques for gene integration. This technique has gained attention in various bacteria, including *Methanosarcina* (43) and *Mycobacterium smegmatis* (44), due to its simple design and high efficiency (45, 46). The  $\varphi$ C31 phage recombinase is commonly utilized due to its ability to function independently of a helper protein, and the recombination is unidirectional (47). For example, in *Clostridium ljungdahlii*, a whole butyric acid synthesis pathway was integrated into its genome by  $\varphi$ C31 recombinase (45). In *Methanosarcina* spp., the  $\varphi$ C31 recombinase achieved genome editing efficiency that is 30 times higher than that of homologous recombination (43) .

Among many value-added chemical products obtained from advanced genome engineering tools, bioplastics from microorganisms have become an attractive product (reviewed in (48)). This is particularly pertinent due to the detrimental environmental impact of excessive plastic usage in recent years. Bioplastics preserve the advantageous properties of petroleum-based plastics, such as high durability, moldability, water, and heat resistance, while also offering biocompatibility, emerge as a promising alternative (49–51). Moreover, numerous microorganisms possess the natural ability to degrade bioplastics, including the polyhydroxyalkanoate (PHA) family, either aerobically or anerobically, typically within a span of 5 to 6 weeks (50–52). However, the high feedstock cost remains an obstacle to the bioplastic's competitiveness in the market (reviewed in (53, 54)). This issue can be addressed by using photoautotrophic microbes that can use cheap alternatives and waste feedstock (such as CO<sub>2</sub>) (27).

PHA stands out as the most extensively studied bioplastic (48, 54). The PHA pathway consists mainly of *phaA*, *phaB*, *phaC*, and *phaZ* genes. *phaA* encodes a ß-keto thiolase, while *phaB* encodes an acetoacetyl-CoA reductase (27). PhaC catalyzes the polymerization of PHA, whereas PHA depolymerase, PhaZ, catalyzes its mobilization during carbon starvation (27). Additional proteins, such as PhaP and PhaR, have also been reported to contribute to the maturation and regulation of PHA granules (55, 56). In *Paracoccus denitrificans*, PhaR is characterized as a repressor of PHA synthesis and acts by binding to the intergenic region of the *phaC-phaP* and *phaP-phaR* genes (55). However, PhaR is proposed to be an activator for PHA synthesis in *Cupriavidus necator* in a PhaP-dependent and -independent manner. Deletion of the *phaR* gene decreased PHA production in this organism (56). We have previously reported that TIE-1 possesses one *phaR* gene (Rpal\_0531) using bioinformatics (27).

To improve PHA production, several gene manipulations have been undertaken directly on PHA pathway genes or genes from other pathways that may impact or compete with the PHA biosynthesis pathway (57–59). For instance, a study revealed that the deletion of the *phaZ* gene in *Sinorhizobium meliloti* increased PHA production compared to wild-type when utilizing formate generated through electrochemical CO<sub>2</sub> reduction (57). This suggests that prevention of PHA degradation results in intracellular accumulation of PHA. Metabolic pathways such as glycogen production and nitrogen fixation are also potential competitors for bacterial PHA production (58). In *Synechocystis* sp. PCC 6803, PHA accumulation is reported to be linked to glycogen production under prolonged nitrogen starvation conditions. Mutants lacking the glycogen phosphorylase genes showed impaired PHA accumulation, supporting the link between glycogen and PHA synthesis under nitrogen starvation (NaNO<sub>3</sub>) conditions (58). Nitrogen fixation, which is a pathway highly demanding of electrons, could also present another competition to PHA production (60). Furthermore, PHA accumulation has also been reported to be induced by nitrogen deprivation ((N<sub>2</sub>) or NH<sub>4</sub>Cl) in many bacteria (41, 61, 62).

In another study, increase in PHA production was achieved by enhancing carbon fixation through the Calvin–Benson–Bassham (CBB) cycle in *Ralstonia eutropha* (now *C. necator*) (60). This enhancement involved the heterologous overexpression of the RuBisCO gene from *Synechococcus sp.* PCC 7002 in *Ralstonia eutropha*. Consequently, the overexpression resulted in a substantial increase in cell density, measured by optical

density, by up to 89.2%. Additionally, there was a significant augmentation of the mass percent of PHA production, reaching up to 99.7% (60).

In this study, we used the  $\varphi$ C31 integration system to integrate additional copies of the RuBisCO form I and II genes driven by the  $P_{aphII}$  constitutive promoter into the TIE-1 genome. Additionally, to increase PHA accumulation in TIE-1, we created mutants that lack key genes in the PHA pathway, particularly focusing on the phaZ and the phaR genes. The behavior of the mutants lacking the phaR helped us elucidate whether phaR is an activator or repressor of the PHA pathway in TIE-1. In addition to exploring genes within the PHA pathway, we also examined the impact of deleting genes in pathways that might potentially compete with the PHA synthesis pathway. These include the mutants that have been previously studied in biobutanol production in the TIE-1:  $\Delta q l y$  mutant lacking glycogen synthase and the mutant lacking the two NifA regulators nifA, Rpal\_1624 & Rpal\_5113, of the nitrogen fixation pathway of TIE-1 (37). We also hypothesize that like R. eutropha, overexpressing RuBisCO genes (form I and II) in TIE-1 could increase intracellular carbon abundance and hence increase PHA accumulation. We tested PHA production in all six strains and wild-type under a variety of growth conditions, including non-nitrogen-fixing conditions with NH<sub>4</sub>Cl (referred to as non-nitrogen-fixing conditions throughout) and nitrogen-fixing conditions with N2 gas (referred to as nitrogen-fixing conditions throughout).

Our results show that the deletion of the *phaR* gene increased PHA production (dry cell weight % wt/wt) when TIE-1 was grown photoheterotrophically with butyrate under non-nitrogen-fixing conditions. We also observed an increase in PHA production (dry cell weight % wt/wt) from the  $\Delta gly$  and  $\Delta nifA$  under photoautotrophic growth conditions with H<sub>2</sub> and under non-nitrogen-fixing conditions. PHA production increased in TIE-1 strains overexpressing RuBisCO form I and form I & II genes under photoheterotrophy with butyrate irrespective of the nitrogen source used and photoautotrophy with H<sub>2</sub> under non-nitrogen-fixing conditions as well as photoelectrotrophically under nitrogen fixing conditions. We show that both gene deletion and overexpression can enhance PHA production by TIE-1. This work advances TIE-1 as a model organism for potential commercialization for PHA production and provides valuable insights for future genetic engineering endeavors aimed at enhancing bioplastic production in other purple nonsulfur bacteria.

### **RESULTS**

# Generating TIE-1 mutants and suicide plasmids with the different antibiotic markers

To improve polyhydroxyalkanoate (PHA) production, we constructed a mutant lacking the regulator of PHA pathway ( $\Delta phaR$ ) and a mutant lacking PHA depolymerase ( $\Delta phaZ$ ) (Fig. S1 and S2). The mutant lacking the glycogen synthesis gene ( $\Delta gly$ ) as well as the double mutant lacking the nitrogen-fixing regulator *nifA* genes ( $\Delta nifA1 \Delta nifA2$ ; referred as *DnifA* throughout) were constructed previously (37) . These strains are listed in Table 1, and the plasmids used to construct them are listed in Table 2.

All the mutants were constructed by using a suicide plasmid (pJQ200KS) carrying a gentamicin resistance cassette. Using gentamycin has two disadvantages: 1) wild-type TIE-1 has a remarkably high resistance to gentamicin with a minimum inhibitory concentration (MIC) of 200 µg/mL and 2) gentamicin is expensive (65). For enhanced competitiveness in large-scale production of PHA, opting for other antibiotics with lower MIC values than gentamicin could offer a more cost-effective alternative. Accordingly, we constructed suicide plasmids containing two widely used antibiotic resistance markers: chloramphenicol (MIC of 100 µg/mL) or kanamycin (MIC of 50 µg/mL), using pJQ200KS as the backbone, as listed in Table 2 and shown in Fig. S3.

TABLE 1 Strains used in this study

Strain	Relative characteristics	Function	Source
AB415	Wild-type Rhodopseudomonas palustris TIE-1	Wild-type TIE-1	(26)
WB065	Wild-type TIE-1 with attB	For designing RuBisCO strains	This study
WB068	Wild-type TIE-1 with φC31 integrase; P <sub>lac</sub> ; laclq; attB	For designing RuBisCO strains	This study
WB090	Wild-type TIE-1 with mCherry; Paphll promoter; fd terminator; attL; attR	For designing RuBisCO strains	This study
WB091	Wild-type TIE-1 with <i>loxp-mCherry-loxp</i> ; <i>Paphll</i> promoter; <i>fd</i> terminator; <i>attL</i> ; <i>attR</i>	For designing RuBisCO strains	This study
AB188	TIE-1 $\Delta gly$ mutant	TIE-1 mutant lacking the glycogen synthase gene	(37), this study
AB187	TIE-1 Δ <i>nifA</i> double mutant	TIE-1 mutant lacking the <i>nifA</i> <sub>1&amp;2</sub> genes	(37), this study
AB186	ΔphaR	TIE-1 mutant lacking the phaR gene	This study
\B189	ΔphaZ	TIE-1 mutant lacking the phaZ gene	This study
AB199	Wild-type TIE-1 with RuBisCO form I gene overexpressed	Engineered TIE-1 for PHA overproduction	This study
AB200	Wild-type TIE-1 with RuBisCO form I and II genes overexpressed	Engineered TIE-1 for PHA overproduction	This study

# Engineering TIE-1 using a phage integration system to increase PHA production in TIE-1

As previously discussed, homologous recombination presents a time-intensive process and remains so far the only successful genetic tool for TIE-1. To address these challenges, we devised a phage integration system for incorporation of genes into its genome. Fig. 1 delineates the essential components of the  $\phi$ C31 recombinase system: the *attB* site, *attP* site, and the  $\phi$ C31 integrase.

To compensate for the lack of an *attB* site in TIE-1, we inserted it into the genome, as described in Materials and Methods. The *attP* site was introduced into a suicide plasmid with a constitutively expressed *mCherry* gene under the  $P_{aphII}$  promoter (pWB081). For the expression of  $\varphi$ C31 integrase, the optimal way would be to use a temperature-sensitive plasmid (66). After the targeted genome editing, the removal of the  $\varphi$ C31 integrase could be conveniently executed using this approach. Unfortunately, there is no known temperature-sensitive plasmid that replicates in TIE-1. Hence, we decided to build two different systems: (1) a plasmid-based system, where the integrase is introduced into TIE-1 by a plasmid (Fig. 1B), and (2) a genome-based system, where the integrase is

TABLE 2 Plasmids used in this study

Plasmid	Relative characteristics	Source
pJQ200KS	ori <i>P15A</i> ; Gen <sup>r</sup>	(63)
pAB314	pJQ200KS with GImUSX_UP and GImUSX_DN	(34)
pAB356	Cm <sup>r</sup>	(64)
pAB357	Kan <sup>r</sup>	(64)
pAB358	Tc <sup>r</sup>	(64)
pAB359	Amp <sup>r</sup>	(64)
pSRKGm	P <sub>lac</sub> ; laclq; ori pBBR1; Gen <sup>r</sup>	(64)
pWB083	pAB314 with attB	This study
pWB081	pJQ200KS with mCherry; Paphil promoter; fd terminator and attP	This study
pWB084	pSRKGm with φ <i>C31</i> integrase	This study
pWB086	pAB314 with φC31 integrase; P <sub>lac</sub> ; laclq; attB	This study
pWB088	pJQ200KS with φC31 integrase; PaphII promoter; fd terminator and attP	This study
pWB091	pJQ200KS with Kan <sup>r</sup>	This study
pWB092	pJQ200KS with Cm <sup>r</sup>	This study
pWB107	RuBisCO form I and form II gene overexpression	This study
pWB108	RuBisCO form I gene overexpression	This study
pAB863	pJQ200KS with <i>phaR</i> 1 kb up and 1 kb down for deletion of <i>phaR</i>	This study
pAB868	pJQ200KS with <i>phaZ</i> 1 kb up and 1 kb down for deletion of <i>phaZ</i>	This study

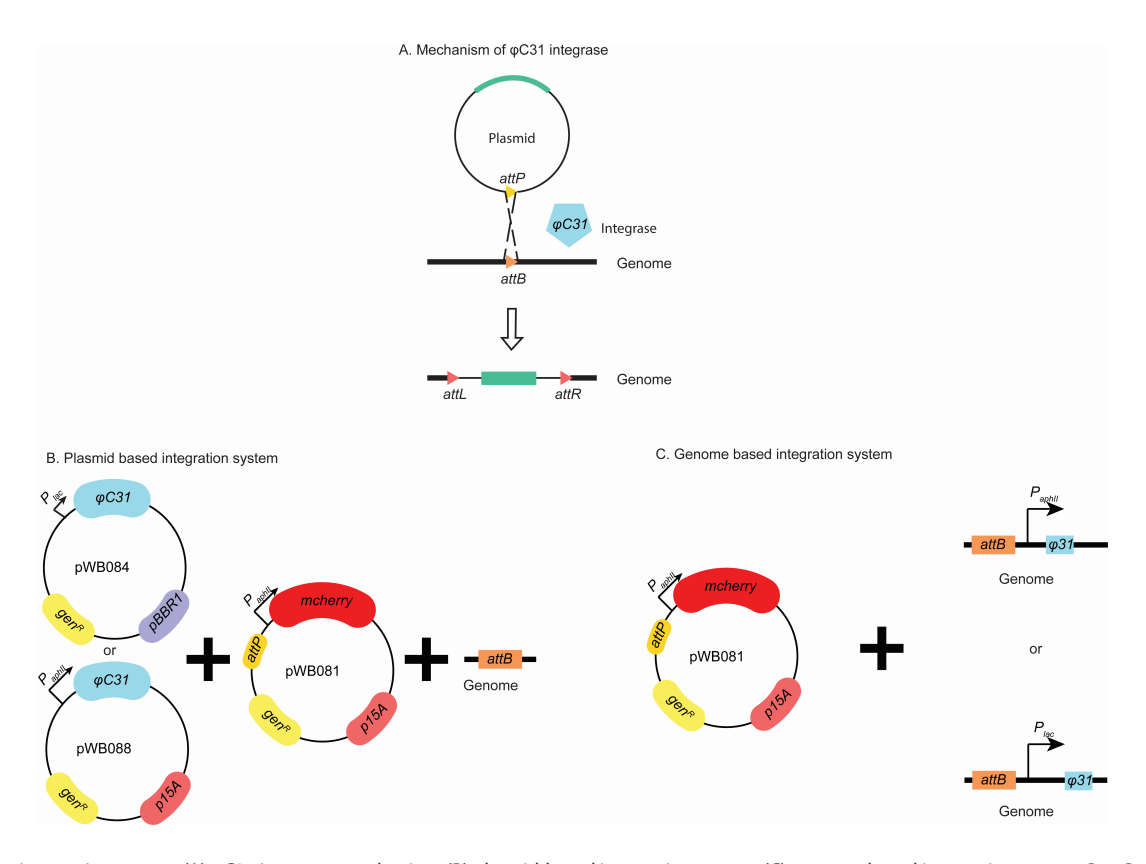


**FIG 1** Phage integration system. (A)  $\varphi$ C31 integrase mechanism; (B) plasmid-based integration system; (C) genome-based integration system.  $P_{lao}$  Promoter;  $P_{$ 

integrated into the TIE-1 genome (Fig. 1C). The advantage of the plasmid-based system is its mobility, while the genome-based system is more stable and does not rely on antibiotics. Both an inducible promoter ( $P_{lac}$ ) and a strong constitutive promoter ( $P_{aphll}$ ) were tested. To summarize, as shown in Fig. 1, we have four different designs for the expression of the  $\varphi$ C31 integrase: a)  $P_{aphll}$ -driven  $\varphi$ C31 integrase on a suicide plasmid (pWB088); b)  $P_{lac}$ -driven  $\varphi$ C31 integrase on a self-replicating plasmid (pWB084); c)  $P_{aphll}$ -driven  $\varphi$ C31 integrase on the TIE-1 genome (Fig. 1C(a)); and d)  $P_{lac}$ -driven  $\varphi$ C31 integrase on the TIE-1 genome (Fig. 1C(a)). After three separate trials, we were not able to obtain a genome-based system using the constitutive promoter (Fig. 1C(a)). Thus, we only present the results of the other three systems. The successful integration of mCherry was indicated by visualizing red fluorescence at an emission wavelength of 610 nm.

Upon confirming integration, we assessed the efficiency of the various systems by measuring the transformation efficiency (detailed calculation described in Materials and Methods) and the integration efficiency, which is defined as the percentage of colonies that have red fluorescence signals among all obtained colonies. As shown in Fig. 2A and B, the transformation efficiency normalized to the plasmid concentration is higher for the genome-based system (P < 0.001) (Fig. 1C). This higher efficiency could be due to the sufficiency of only one plasmid for the system to be functional. Between the two plasmid-based systems, the constitutively expressed  $\phi$ C31 reached higher efficiency (Fig. 1B, pWB088). This higher efficiency could be due to the independence from the use of the inducer, IPTG. For the integration frequency, the genome-based system (Fig. 1C) and the plasmid-based system both with the constitutive promoter (Fig. 1B, pWB088) and inducible promoter resulted in similar editing efficiencies between 80% and 100% (P = 0.13) (Fig. 2B). To summarize, the genome-based system with an inducible promoter results in highest transformation efficiency, while all three systems have similar editing efficiencies.

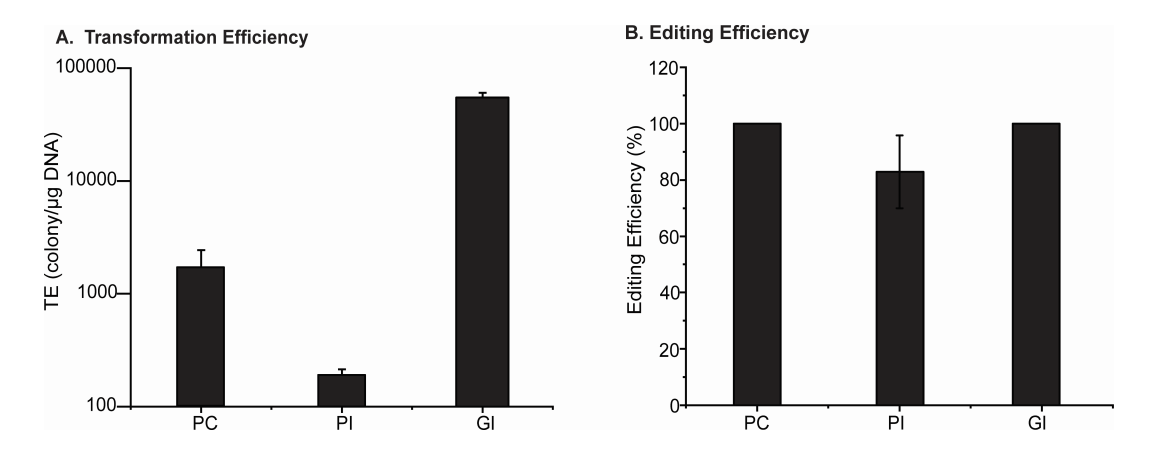


FIG 2 (A) Transformation efficiency normalized to the plasmid amount. (B) Editing efficiency. TE, transformation efficiency; PC, plasmid-based system with the constitutive promoter; PI, plasmid-based system with the inducible promoter.

After successfully integrating mCherry, we wanted to use the phage integration tool to assist in improving PHA production in TIE-1. Previous research conducted on Ralstonia eutropha (now Cupriavidus necator) has shown that overexpression of RuBisCO resulted in improved PHA production (60). Thus, to improve PHA production, we integrated a  $P_{aphll}$  -driven RuBisCO form I alone or RuBisCO form I and form II together into the TIE-1 genome to obtain two new TIE-1 strains:  $\Omega rub(I)$  and  $\Omega rub(I|\&II)$ . We were unable to obtain a plasmid with  $P_{aphll}$  -driven RuBisCO form II only. The successful integration of these genes and  $P_{aphll}$  was analyzed by PCR amplification of the  $P_{aphll}$  region and the RuBisCO gene form I and II, as indicated in Fig. S4. In addition, the whole genome of each constructed strain has been sequenced.

# Deletion of *phaR*, *phaZ*, or overexpression of the RuBisCO form I impaired the growth of TIE-1 during photoheterotrophic growth with butyrate

Because TIE-1 has previously exhibited high PHA production under anoxic photoheterotrophic conditions with butyrate (27), we evaluated this growth condition using all the constructed strains. Under these anoxic growth conditions, light is used as an energy source and butyrate is used both as an electron and a carbon source. For all growth conditions explored, we determined the effect of nitrogen fixation by supplying N<sub>2</sub> gas (nitrogen-fixing) or ammonium chloride (NH<sub>4</sub>Cl) salt (non-nitrogen-fixing). The growth parameters were obtained both from 1 mM (shown in Table 3; Fig. 3A and B) and 10 mM (shown in Table S1) butyrate. A 1 mM concentration was chosen to allow a clear growth trend without reaching saturation of the OD<sub>660</sub>. To collect enough biomass, PHA production was only obtained from growth with 10 mM butyrate. Our results show that the growth with 1 mM butyrate did not reveal a significant difference between the various constructed strains (Fig. 3A and B). Deleting phaR or phaZ increased the generation time of TIE-1 by around 3 hours compared to wild-type when grown photoheterotrophically with 10 mM butyrate under non-nitrogen-fixing conditions (Table S1) (P = 0.01). However, a slightly shorter generation time (around 3 hours shorter than that of wild-type) was obtained from the  $\Delta gly$  and the  $\Delta nifA$ under these conditions (Table S1) (P = 0.007). Under nitrogen-fixing conditions, the AphaZ mutant continued to show a growth defect observed as a longer generation time (3 hours longer than wild type), whereas the  $\Delta phaR$  and  $\Delta gly$  mutants showed the same generation time as that of wild-type (Table S1). As expected,  $\Delta nifA$  was not able to grow under nitrogen-fixing conditions (Table 3; Table S1; Fig. 3B). We compared the growth of the engineered RuBisCO strains  $\Omega rub(I)$  and  $\Omega rub(I|MI)$  under the same photoheterotrophic growth condition with butyrate. The engineered strain carrying only the overexpressed RuBisCO gene form I  $(\Omega rub(I))$  has a growth defect under both nitrogen-fixing and non-nitrogen-fixing conditions with 10 mM butyrate (Table S1), as

TABLE 3 Growth parameter values of the knockout and engineered TIE-1 strains grown under different growth conditions

	ΔphaR	۵	ΔphaZ	2	4919	_	Dully	7	(I)anzs	r	szrup(IœII)	L	- ^
Generation time G (h)													
But (NH <sub>4</sub> Cl)	6.58 (0.34)	0.39	5.45 (0.42)	0.00	6.81 (0.18)	96.0	6.58 (0.37)	0.40	6.79 (0.13)	0.92	6.49 (0.36)	0.25	6.80 (0.20)
But (N <sub>2</sub> )	10.18 (0.52)	0.002	9.57 (0.34)	0.002	8.03 (1.42)	0.99	NG	NG	8.48 (0.84)	0.42	7.0 (0.79)	0.094	8.04 (0.22)
H <sub>2</sub> (NH <sub>4</sub> CI)	14.98 (1.32)	0.01	13.20 (0.54)	0.00	9.74 (0.4)	0.442	11.16 (0.71)	0.154	9.7 (0.3)	0.37	10.51 (4.25)	0.89	10.14 (0.71)
H <sub>2</sub> (N <sub>2</sub> )	88.80 (27.78)	0.52	64.90 (9.2)	0.36	75.29 (12.74)	0.971	NG	ŊĊ	149.9 (67.03)	0.13	99.77 (36.01)	0.35	75.74 (15.84)
Fe(II) (NH <sub>4</sub> CI)	595 (30.31)	0.65	4620 (2000.5)	0.03	280.71 (57.66)	0.021	369.35 (115)	0.076	740.67 (265)	0.61	644.36 (119)	0.98	641.67 (160)
Fe(II) (N <sub>2</sub> )	ND	ND	NG	SN	235.14 (55.63)	0.498	NG	NG	371.49 (11.7)	0.004	205.33 (155)	0.57	262.1 (29.13)
PE (NH <sub>4</sub> CI)	517.3 (48.1)	0.21	1212.75 (173.2)	0.0048	1008 (0)	0.016	822.9 (86.6)	0.0001	605.02 (3.49)	0.18	337.41 (10.7)	0.40	262.32 (9.11)
PE (N <sub>2</sub> )	646.8 (0)	0.71	3482.73 (3211)	0.28	42446.2 (84892)	0.37	NG	ŊĊ	1060.8 (105)	0.54	4207 (3316)	0.27	800.25 (115)
Maximum OD <sub>660</sub>													
But (NH <sub>4</sub> CI)	0.78 (0.07)	0.35	0.86 (0.04)	0.22	0.81 (0.06)	0.79	0.89 (0.01)	0.00	0.71 (0.06)	0.03	0.69 (0.03)	0.00	0.82 (0.01)
But (N <sub>2</sub> )	0.653 (0.04)	0.036	0.67 (0.04)	0.113	0.70 (0.02)	0.107	NG	ŊĊ	0.78 (0.05)	0.32	0.80 (0.07)	0.28	0.74 (0.03)
H <sub>2</sub> (NH₄CI)	2.48 (0)	0.001	2.495 (0.01)	0.001	1.36 (0.28)	0.454	1.64 (0.24)	0.12	1.98 (0.742)	0.26	2.22 (0.403)	0.07	1.17 (0.071)
H <sub>2</sub> (N <sub>2</sub> )	1.73 (0.19)	0.642	1.963 (0.19)	0.11	1.89 (0.42)	0.409	NG	ŊĊ	1.73 (0.239)	0.68	1.3 (0.482)	0.31	1.65 (0.19)
Fe(II) (NH <sub>4</sub> CI)	0.04 (0)	0.002	0.021 (0)	0.016	0.14 (0.008)	0.00	0.082 (0)	0.00	0.11 (0.012)	0.00	0.03 (0.001)	0.01	0.03 (0.0017)
Fe(II) (N <sub>2</sub> )	0.02 (0.01)	0.013	NG	NG	0.10 (0.02)	0.977	NG	NG	0.06 (0.002)	0.09	0.11 (0.029)	0.85	0.09 (0.012)
PE (NH <sub>4</sub> CI)	0.27 (0.00)	0.332	0.160 (0.00)	0.029	0.17(0)	0.036	0.17 (0.00)	0.035	0.26 (0.006)	0.29	0.29 (0.001)	0.34	0.38 (0.003)
PE (N <sub>2</sub> )	0.39 (0.005)	0.218	0.19 (0.00)	0.944	0.098 (0.002)	0.01	NG	NG	0.16 (0.002)	0.46	0.122 (0)	0.04	0.19 (0.001)
Time to reach maximum OD (h)													
But (NH <sub>4</sub> CI)	98 (0.00)	0	0 114 (0.00)	0	74 (0.00)	0	74 (0.00)	0	82 (0.00)	0	74 (0.00)	0	74 (0.00)
But (N <sub>2</sub> )	122 (0)	0.0065	122.33 (0)	0.000	114(0)	0	NG	ŊĊ	130 (0)	0	114 (0)	0	(0) 86
H <sub>2</sub> (NH₄CI)	90.5 (0.71)	0.00	290.5 (0.70)	0.00	338.5 (0.71)	_	338.5 (0.71)	-	243 (135.76)	0.42	338.5 (0.71)	_	338.5 (0.71)
H <sub>2</sub> (N <sub>2</sub> )	472.67 (0.58)	_	472.7 (0.57)	<del>-</del>	472.67 (0.58)	_	NG	NG	472.67 (0.58)	-	472.67 (0.58)	_	472.67 (0.58)
Fe(II) (NH <sub>4</sub> CI)	1680.33 (0.5)	0.00	1680.2 (0.29)	0.00	1320.33 (0.58)	0.00	1320.67 (1.1)	0	1319.67 (0.5)	0.00	936.33 (0.58)	0.23	935.67 (0.58)
Fe(II) (N <sub>2</sub> )	1704.33 (0.5)	0.00	NG	NG	1200.33 (0.58)	_	NG	ŊĊ	671.67 (0.58)	0.00	1200.33 (0.5)	0.37	1200.33 (0.58)
PE (NH <sub>4</sub> CI)	336 (0)	0.00	336 (0)	0.00	336 (0)	0.00	336 (0)	0.00	336 (0)	0.00	336 (0)	0.00	336 (0)
PE (N <sub>2</sub> )	336 (0)	0.00	336 (0)	0.00	336(0)	0.00	NG	DN	336 (0)	0.00	336 (0)	0.00	336 (0)
Lag time (h)													
But (NH <sub>4</sub> Cl)	10.80 (0.23)	0.00	10.92 (0.71)	0.00	10.11 (1.10)	0.11	10.77 (0.28)	0.00	14.32 (2.72)	0.00	11.52 (2.00)	0.022	9.02 (0.36)
But (N <sub>2</sub> )	17.06 (0.33)	0.0051	17.56 (0.10)	0	17.26 (1.75)	0.14	NG	NG	19.22 (0.82)	0.0019	0.0019 16.56 (0.96)	0.12	15.4 (0.39)
H <sub>2</sub> (NH <sub>4</sub> CI)	94.03 (22.7)	0.1454	84.97 (1.66)	0.009	81.14 (1.5)	0.011	73.59 (5.47)	0.063	73.57 (10.03)	0.14	89.87 (3.64)	0.01	56.25 (3.45)
H <sub>2</sub> (N <sub>2</sub> )	267.23 (123)	0.21	192 (13.97)	0.103	191.1 (20)	0.143	NG	DN	185.85 (69.6)	0.55	115.83 (27.5)	0.11	158.82 (23.3)
Fe(II) (NH <sub>4</sub> CI)	ND	ND	ND	ND	416.54 (27.27)	0.366	805.62 (165)	0.0218	3 706.5 (13.28)	0.01	296.7 (11.71)	8.0	321.34 (159)
Fe(II) (N <sub>2</sub> )	ND	ND	Ŋġ	NG	919.89 (146.9)	0.874	NG	SN	714.13 (60.7)	0.008	792.07 (194)	0.376	905.17 (33.2)

ουννιι μαιαιπετετ sotrained from 1 mM butyrate. Values are averages from biological triplicates. Standard error values are in parentheses. P, values against wild-type values. P values in bold indicate statistical significance. But, butyrate, Fe, iron; NH<sub>4</sub>Cl, ammonium chloride; N<sub>2</sub>, nitrogen gas; NG, no growth; ND, not determined—almost close to the whole growth time. Final OD obtained from 14 days of growth under PE was reported as max OD.

Downloaded from https://journals.asm.org/journal/aem on 01 July 2025 by 75.133.168.157.

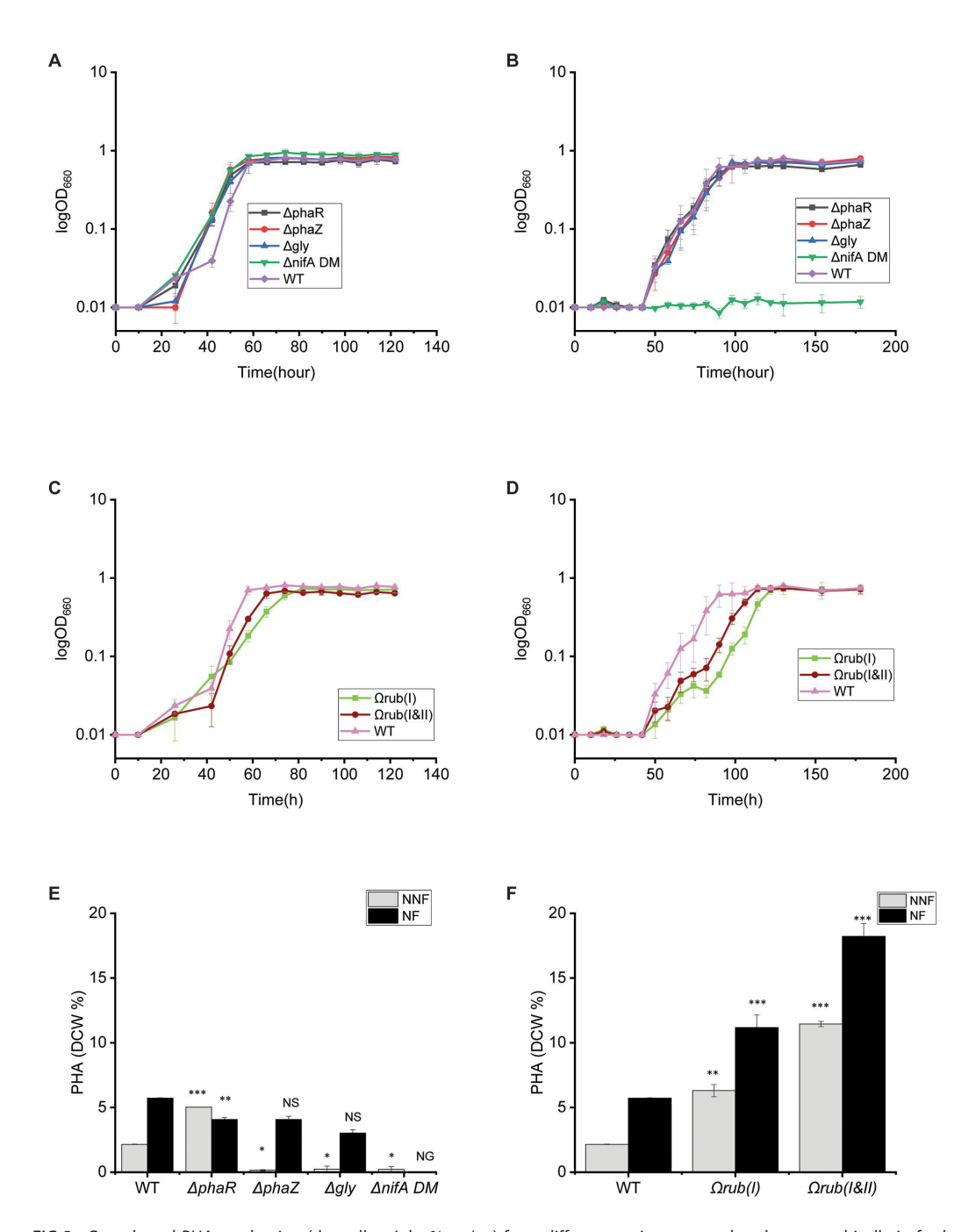


FIG 3 Growth and PHA production (dry cell weight % wt/wt) from different strains grown photoheterotrophically in fresh water basal media with butyrate. (A) Growth of all mutant strains under non-nitrogen-fixing conditions. (B) Growth of all mutant strains under nitrogen-fixing conditions. (D) Growth of all the RuBisCO engineered strains under nitrogen-fixing conditions. (E) PHA production from mutants and TIE-1 strains grown with butyrate under non-nitrogen-fixing and nitrogen-fixing conditions. (F) PHA production from the RuBisCO engineered and wild-type TIE-1 strains grown with butyrate under non-nitrogen-fixing and nitrogen-fixing conditions. NFF = non-nitrogen-fixing; NN = nitrogen-fixing. Error bars from growth curves represent the standard deviation calculated from three replicates, while error bars from PHA production depict the standard error derived from biological triplicates. The statistical differences in PHA production were calculated using two-tailed Student's test against wild-type TIE-1.  $*P \le 0.05, **P < 0.01,$  and \*\*\*P < 0.001; NS, not significant; ND, not detected; NG, no growth.

well as with 1 mM butyrate (Table 3). This defect seems to be more noticeable under nitrogen-fixing growth conditions. The  $\Omega rub(l)$  strains have an ~2X (P = 0.01) longer lag

time than wild-type strains when grown photoheterotrophically with 10 mM butyrate under non-nitrogen-fixing conditions, and ~5X (P = 0.001) longer generation time under nitrogen-fixing conditions (Table S1). Lag time was also about 4 hours longer (P = 0.001) when the  $\Omega rub(I)$  was grown with only 1 mM butyrate both under nitrogen and non-nitrogen-fixing conditions (Table 3).

The engineered strain  $\Omega rub(l\&ll)$  carrying overexpressed RuBisCO form I and II genes did not show any significant differences in growth compared to wild-type strains when grown under non-nitrogen-fixing or under nitrogen-fixing conditions (Table S1; Table 3; Fig. 3C and D).

# Deletion of the *phaR* gene or overexpression of the RuBisCO form I and II genes increases PHA production in TIE-1 under photoheterotrophic growth with butyrate

Deletion of the *phaR* (regulator gene) increased PHA production (mg/L/cell and dry cell weight % wt/wt) ~2X (P=0.00) compared to wild-type under non-nitrogen-fixing or nitrogen-fixing conditions (Fig. 3E; Table 4; Table S2). Deletion of the *phaZ*, *gly*, or *nifA* genes resulted in an overall decrease in PHA production (mg/L/cell and dry cell weight % wt/wt) of ~10X (P=0.05) compared to wild-type under growth under non-nitrogen-fixing conditions. These deletions did not seem to affect PHA production when compared to wild-type under nitrogen-fixing conditions. We did not detect any PHA from the  $\Delta$ nifA grown under nitrogen-fixing conditions as it did not show any growth. Except for  $\Delta$ phaR, all strains exhibited a consistent increase in PHA production during nitrogen-fixing growth conditions in comparison to growth under non-nitrogen-fixing conditions.

When grown photoheterotrophically with butyrate, the two strains harboring the  $\Omega rub(l)$  and  $\Omega rub(l\&l)$  demonstrated increased PHA production, regardless of the nitrogen source. Under non-nitrogen-fixing conditions, the  $\Omega rub(l)$  strain had 2X (P=0.00) higher PHA production (mg/L/cell and dry cell weight % wt/wt) than wild-type, while the  $\Omega rub(l\&l)$  exhibited a 5X increase (P=0.001). This increase in PHA was also observed under nitrogen-fixing conditions where an increase of 1.9X (P=0.007) was observed from the  $\Omega rub(l)$  and 3X (P=0.001) from the  $\Omega rub(l\&l)$  (Fig. 3F; Table 4; Table S2). Like the deletion mutants, an overall increase in PHA production was observed from the engineered and wild-type strains under nitrogen-fixing vs non-nitrogen-fixing conditions (Fig. 3F).

# Deletion of the *phaR*, *phaZ*, or overexpression of RuBisCO form I and II genes increased the final optical density of TIE-1 under photoautotrophic growth with $\rm H_2$ under non-nitrogen-fixing conditions

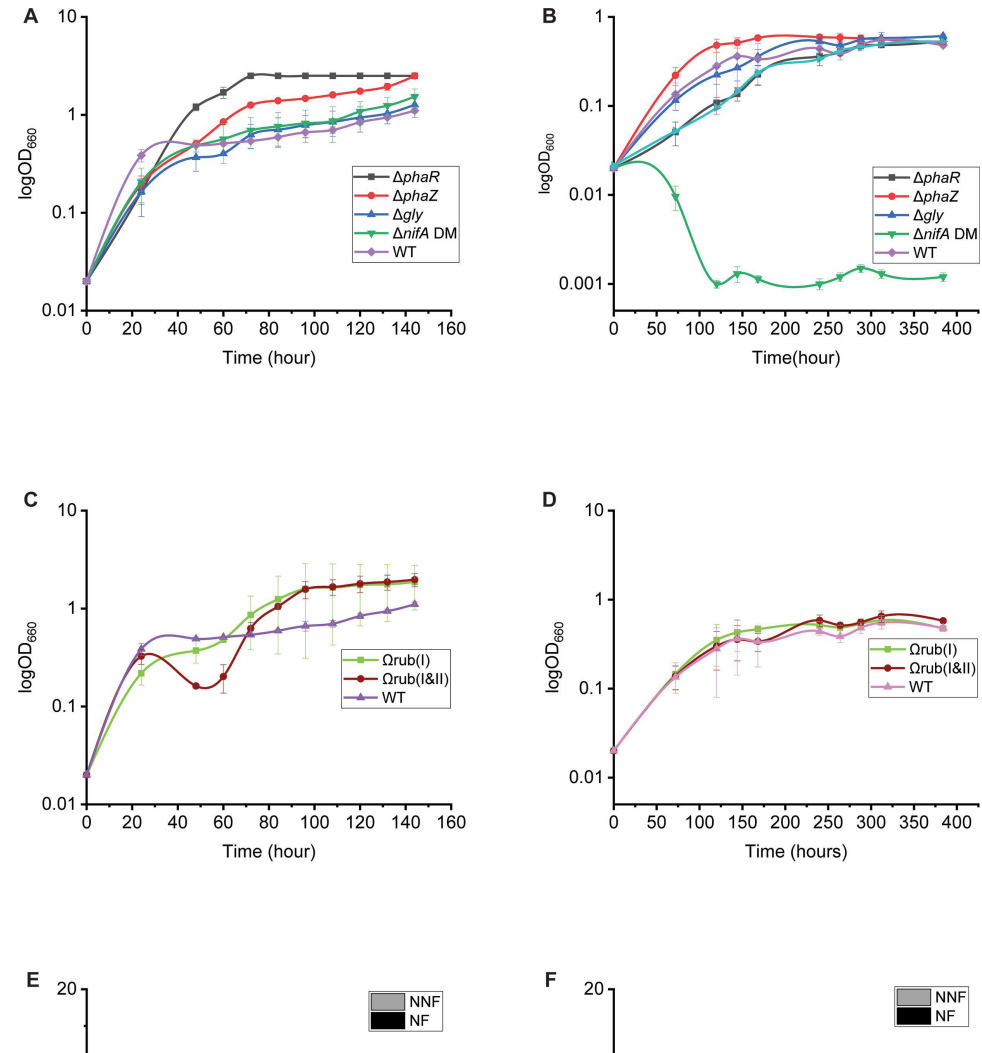
Achieving production from a low-cost and abundant carbon source is one of the most impactful pathways for bioplastic production. Accordingly, we tested the growth of all the strains under photoautotrophic conditions using H<sub>2</sub> as an electron source and CO<sub>2</sub> as a carbon source in a freshwater basal liquid medium. Light is used as the energy source as TIE-1 is a photosynthetic bacterium. Fig. 4A; Table 3 show that although  $\Delta phaR$  and  $\Delta phaZ$  mutants showed a slightly longer generation time (~3 hours slower) (P=0.001) , they reached the maximum OD faster than wild-type strains when grown with H<sub>2</sub> under non-nitrogen-fixing conditions.

Although the strains  $\Omega rub(l\&l)$  showed an extended lag time (1.6 X slower than wild-type P=0.01), they reached a higher final OD (0.52 higher) than wild-type (Table 3) when grown with  $H_2$  and under non-nitrogen-fixing conditions. The  $\Omega rub(l)$  did not show any significant growth difference compared to wild-type (Table 3; Fig. 4C). No difference was observed between the two engineered strains when grown with  $H_2$  under nitrogen-fixing conditions (Table 3; Fig. 4D).

 $\textbf{TABLE 4} \quad \text{PHA production from different TIE-1 strains under photoautotrophic and heterotrophic growth conditions}^{\varrho}$ 

	∆phaR	Ь	∆phaZ	Ь	$\Delta gly$	Ь	ΔnifA	Ь	Ωrub(I)	Ь	Ωrub(I&II)	Ь	WT
PHA (mg/L)													
Butyrate (NH <sub>4</sub> CI)	30.37 (0.33)	0.03	4.86 (0.69)	0.116	5.25 (0.67)	0.098	8.21 (0.3)	0.29	36.03 (1.61)	0.003	41.1 (0.52)	0.016	12.061 (0.27)
Butyrate (N <sub>2</sub> )	14.3 (0.46)	0.003	13.73 (1.68)	0.001	15.87 (1.36)	0.07	NG	NG	49.71 (4.88)	0.002	53.23 (2.91)	0	25.138 (0.05)
H <sub>2</sub> (NH <sub>4</sub> CI)	24.45 (2.08)	0.349	24.51 (1.33)	0.387	29.18 (0.14)	0.754	34.65 (3.1)	0.58	40.15 (4.25)	0.234	32.8 (3.57)	0.819	31.089 (1.37)
H <sub>2</sub> (N <sub>2</sub> )	32.49 (1.25)	0.505	30.82 (1.21)	0.556	16.09 (0.76)	0.151	NG	NG	32.72 (1.16)	0.655	13.06 (1.16)	0.115	25.757 (0.26)
Fe(II) (NH <sub>4</sub> CI)	1.25 (0.04)	0.013	ND	ND	1.46 (0.04)	0.092	1.7 (0.01)	0.38	1.85 (0.034)	0.374	1.79 (0.075)	0.394	2.19 (0.03)
Fe(II) (N <sub>2</sub> )	0.24 (0.012)	0	0.29 (0.02)	0.002	0.42 (0.008)	0.02	NG	NG	0.28 (0.018)	0.005	0.80 (0.004)	0.663	0.96 (0.03)
PE (NH <sub>4</sub> CI)	0.40 (0.46)	0.0002	1.23 (0.05)	0.000	0.735 (0.18)	0.000	0.59 (0.008)	0.00	0.62 (0.17)	0.000	0.64 (0.037)	0.000	2.57 (0.058)
PE (N <sub>2</sub> )	0.422 (0.096)	0.604	0.82 (0.009)	0.01	0.59 (0.03)	0.14	NG	NG	0.67 (0.17)	0.14	0.33 (0.012)	0.94	0.34 (0.02)
PHA (mg/L/cell) (x10 <sup>-11</sup> )	("												
Butyrate (NH <sub>4</sub> CI)	2.32 (0)	0	0.079 (0.03)	0.051	0.11 (0.03)	0.056	0.1 (0.03)	0.05	2.91 (0.22)	0.007	5.29 (0.1)	0.001	1 (0.01)
Butyrate (N <sub>2</sub> )	1.89 (0.07)	0.02	1.89 (0.23)	909.0	1.4 (0.12)	0.374	NG	NG	5.16 (0.45)	0.00	8.41 (0.47)	0.00	2.65 (0.02)
H <sub>2</sub> (NH <sub>4</sub> CI)	2.17 (0.14)	0.098	2.63 (0.18)	0.127	3.22 (0.01)	0.056	3.47 (0.27)	0	3.58 (0.21)	0.055	3.01 (0.27)	0.012	1.52 (0.04)
H <sub>2</sub> (N <sub>2</sub> )	4.89 (0.22)	0.517	3.84 (0.15)	0.952	1.66 (0.07)	0.098	NG	NG	4.07 (0.18)	0.862	1.74 (0.31)	0.111	3.76 (0.05)
Fe(II) (NH <sub>4</sub> CI)	2.32 (0.06)	0	ND	ND	1.9 (0.05)	0	4.37 (0.03)	0.37	3.36 (0.71)	0.033	5.64 (0.26)	0.98	5.62 (0.09)
Fe(II) (N <sub>2</sub> )	0.85 (0.03)	0.082	0.45 (0.04)	0.004	0.89 (0.03)	0.075	NG	DN	0.35 (0.038)	0.002	0.68 (0.009)	0.111	1.66 (0.08)
PE (NH₄CI)	0.10 (0.02)	900.0	0.5 (0.02)	0.803	0.35 (0.09)	0.085	0.25 (0.00)	0.25	0.18 (0.04)	0.01	0.17 (0.006)	0.005	0.55 (0.006)
PE (N <sub>2</sub> )	0.124 (0.009)	0.89	0.34 (0.023)	0.023	0.49 (0.036)	0.011	DN	NG	0.307 (0.11)	0.05	0.207 (0.007)	0.05	0.11 (0.016)
PHA (dry cell weight % wt/wt)	% wt/wt)												
Butyrate (NH <sub>4</sub> Cl)	5.03 (0.00)	0	0.15 (0.05)	0.05	0.24 (0.23)	0.05	0.22 (0.22)	0.05	6.30 (0.48)	0.007	11.45 (0.20)	0.001	2.15 (0.02)
Butyrate (N <sub>2</sub> )	4.08 (0.15)	0.02	4.075 (0.25)	909.0	3.03 (0.26)	0.374	NG	NG	11.18 (0.98)	0	18.23 (1.00)	0	5.73 (0.03)
$H_2$ (NH <sub>4</sub> CI)	4.70 (0.30)	0.098	5.7 (0.375)	0.127	6.98 (0.02)	0.056	7.53 (0.58)	0	7.75 (0.45)	0.055	6.52 (0.58)	0.012	3.28 (0.08)
H <sub>2</sub> (N <sub>2</sub> )	10.60 (0.48)	0.517	8.325 (0.32)	0.952	3.57 (0.15)	0.098	NG	DN	8.83 (0.38)	0.862	3.75 (0.50)	0.111	8.15 (0.10)
Fe(II) (NH <sub>4</sub> CI)	5.03 (0.14)	0	ND	ND	4.10 (0.13)	0	9.4 8(0.07)	0.37	7.28(1.50)	0.033	12.23 (0.58)	0.98	12.20 (0.20)
Fe(II) (N <sub>2</sub> )	1.86 (0.08)	0.082	0.9825 (0.1)	0.004	1.93 (0.07)	0.075	NG	NG	0.75 (0.80)	0.002	1.48 (0.02)	0.111	3.60 (0.19)
PE (NH <sub>4</sub> CI)	0.22 (0.03)	900.0	1.075 (0.02)	0.803	0.76 (0.18)	0.085	0.53 (0.00)	0.25	0.38 (0.08)	0.01	0.35 (0.01)	0.005	1.18 (0.018)
PE (N <sub>2</sub> )	0.25 (0.00)	0.89	0.725 (0.02)	0.023	1.05 (0.08)	0.011	NG	NG	0.65 (0.24)	0.05	0.43 (0.02)	0.05	0.24 (0.03)

<sup>a</sup>Values are averages from biological triplicates, except for those from photoelectrotrophic (PE) growth conditions, which are duplicates. PHA from growth on butyrate are from 10 mM concentrations. Standard error values are in pold indicate statistical significance. Fe, iron; NH<sub>4</sub>Cl, ammonium chloride; N<sub>2</sub>, nitrogen gas; PE, photoelectrotrophic growth; NG, no growth; ND, not detectable.



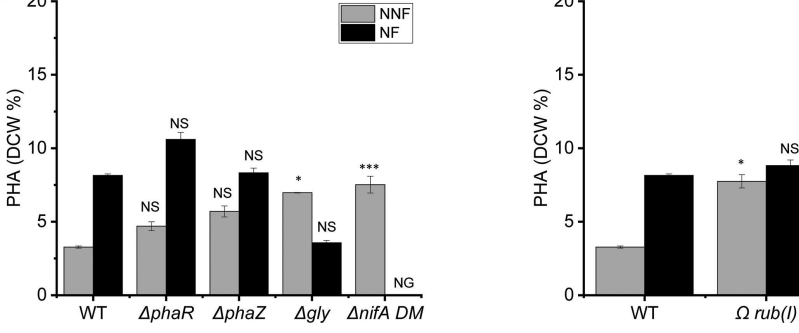


FIG 4 Growth and PHA production (dry cell weight % wt/wt) from different strains grown with fresh water basal media with hydrogen. (A) Growth of all the mutant strains under non-nitrogen-fixing conditions. (B) Growth of all the mutant strains under nitrogen-fixing conditions. (C) Growth of the engineered RuBisCO strains under non-nitrogen-fixing conditions. (D) Growth of all the engineered RuBisCO stains under nitrogen-fixing conditions. (E) PHA production from mutants and TIE-1 wild-type strains grown under non-nitrogen-fixing or nitrogen-fixing conditions. (F) PHA production from Rubisco engineered and wild-type strains grown under hydrogen non-nitrogen-fixing or nitrogen-fixing conditions. NFF, non-nitrogen fixing; NN, nitrogen fixing. Error bars from growth curves represent the standard deviation calculated from three replicates, while error bars from PHA production depict the standard error derived from biological triplicates. The statistical differences in PHA production were calculated using two-tailed Student's test against the wild-type TIE-1. \* $P \le 0.05$ , \*\*P < 0.01, and \*\*\*P < 0.001; NS, not significant; ND, not detected; NG, no growth. Δ*phaR* reached the maximum OD 3.7 X faster than wild-type (P = 0.00) (whereas the Δ*phaZ* mutant reached maximum OD almost 50 hours earlier than wild-type (P = 0.00). Δ*gly* and Δ*nifA* showed similar growth patterns as wild-type under growth with H<sub>2</sub> and non-nitrogen-fixing conditions (Fig. 4A). No significant difference was observed under nitrogen-fixing conditions with hydrogen from all the mutants, except the Δ*nifA*, which showed no growth as shown in Table 3; Fig. 4B.

 $\Omega$  rub(II)

# Deletion of the glycogen synthase (gly), nifA genes, or overexpression of RuBisCO form I or I & II increased PHA production under photoautotrophic growth with H<sub>2</sub> under non-nitrogen-fixing conditions

We tested PHA production (mg/L/cell and dry cell weight % wt/wt) from all the constructed strains under photoautotrophic growth conditions with H<sub>2</sub>. The mutants  $\Delta phaR$  and  $\Delta phaZ$  did not show any significant difference in PHA production compared to wild-type under growth with H<sub>2</sub> regardless of the nitrogen source. The  $\Delta gly$  and the  $\Delta nifA$  strains showed a 2X increase (P=0.05 and P=0, respectively) in PHA production when grown with H<sub>2</sub> under non-nitrogen-fixing conditions (Table 4; Fig. 4E). The deletion of phaR or phaZ did not affect PHA production compared to wild-type strains. No PHA was produced by the  $\Delta nifA$  during growth under nitrogen-fixing conditions due to its inability to grow. Unlike growth with butyrate, switching from non-nitrogen-fixing to nitrogen-fixing conditions increased PHA production only in wild-type TIE-1 but not in the mutants. The mutants showed lower PHA production compared to wild-type under nitrogen-fixing conditions with H<sub>2</sub> as an electron source.

Like growth with butyrate, both engineered  $\Omega rub(l)$  and  $\Omega rub(l\&l)$  strains showed an increase in PHA production (mg/L/cell and dry cell weight % wt/wt) when grown with H<sub>2</sub> under non-nitrogen-fixing conditions. PHA production was nearly double in both engineered strains compared to wild-type (P=0.05 and 0.01, respectively), (Table 4; Fig. 4F). Switching to nitrogen-fixing conditions with H<sub>2</sub> did not affect PHA production (mg/L/cell and dry cell weight % wt/wt) of the two engineered strains  $\Omega rub(l)$  and when compared to wild-type (Table 4; Fig. 4F). In contrast, a decrease in PHA production was observed from the  $\Omega rub(l\&l)$  under nitrogen-fixing conditions (Table 4; Fig. 4F).

# Deletion of the *phaR* and *phaZ* genes impaired the ability of TIE-1 to oxidize Fe(II)

TIE-1 can use electrons produced by the oxidation of Fe(II) for photoautotrophy (photoferrotrophy). Under these difficult growth conditions, the main carbon source is CO<sub>2</sub> and the energy source is light. We tested the growth of all the strains we constructed under photoferrotrophic growth conditions. All the strains were first pre-grown in H<sub>2</sub> to allow the expression of the genes involved in Fe(II) oxidation in TIE-1, as performed previously (27). We observed a defect in the ability of TIE-1 to oxidize Fe(II) and grow when the phaZ or phaR genes were deleted (Fig. 5A and B). Under non-nitrogen-fixing conditions, the phaZ mutant was not able to oxidize Fe(II) or grow even after 50 days (P = 0.003 at day 50 compared to the wild-type). A significant delay in Fe(II) oxidation was observed in the phaR mutant under non-nitrogen-fixing conditions. ΔphaR was able to fully oxidize Fe(II) only after 65 days versus 40 days (P < 0.001 at day 40) for wild-type and grow to wild-type levels. In contrast,  $\Delta q l y$  showed faster Fe(II) oxidation ability, which occurred after 15 days of growth (<0.001 at day 15) as opposed to ~40 days for wild-type when grown under non-nitrogen-fixing conditions. ΔnifA showed a similar iron oxidation pattern as wild-type under non-nitrogen-fixing conditions (Fig. 5A). Under non-nitrogen-fixing conditions, the oxidation ability of  $\Delta gly$  was similar to that of the wild-type. As expected, no Fe(II) oxidation occurred from  $\Delta nifA$  as the strain was not able to grow under nitrogen-fixing conditions. Overexpression of RuBisCO form I appears to delay the ability of TIE-1 to oxidize Fe(II) under non-nitrogen-fixing conditions. However, when RuBisCO form I and II genes are both overexpressed, the strain oxidizes Fe(II) at the same time as wild-type (~40 days) (Fig. 5C). During nitrogen fixation, the  $\Omega rub(l)$ showed faster Fe(II) oxidation compared to wild-type (P < 0.001 at ~day 30), whereas the  $\Omega rub(l\&l)$  initiated Fe(II) oxidation at the same time as wild-type (P = 0.42 at  $\sim day 30$ ), (Fig. 5D).

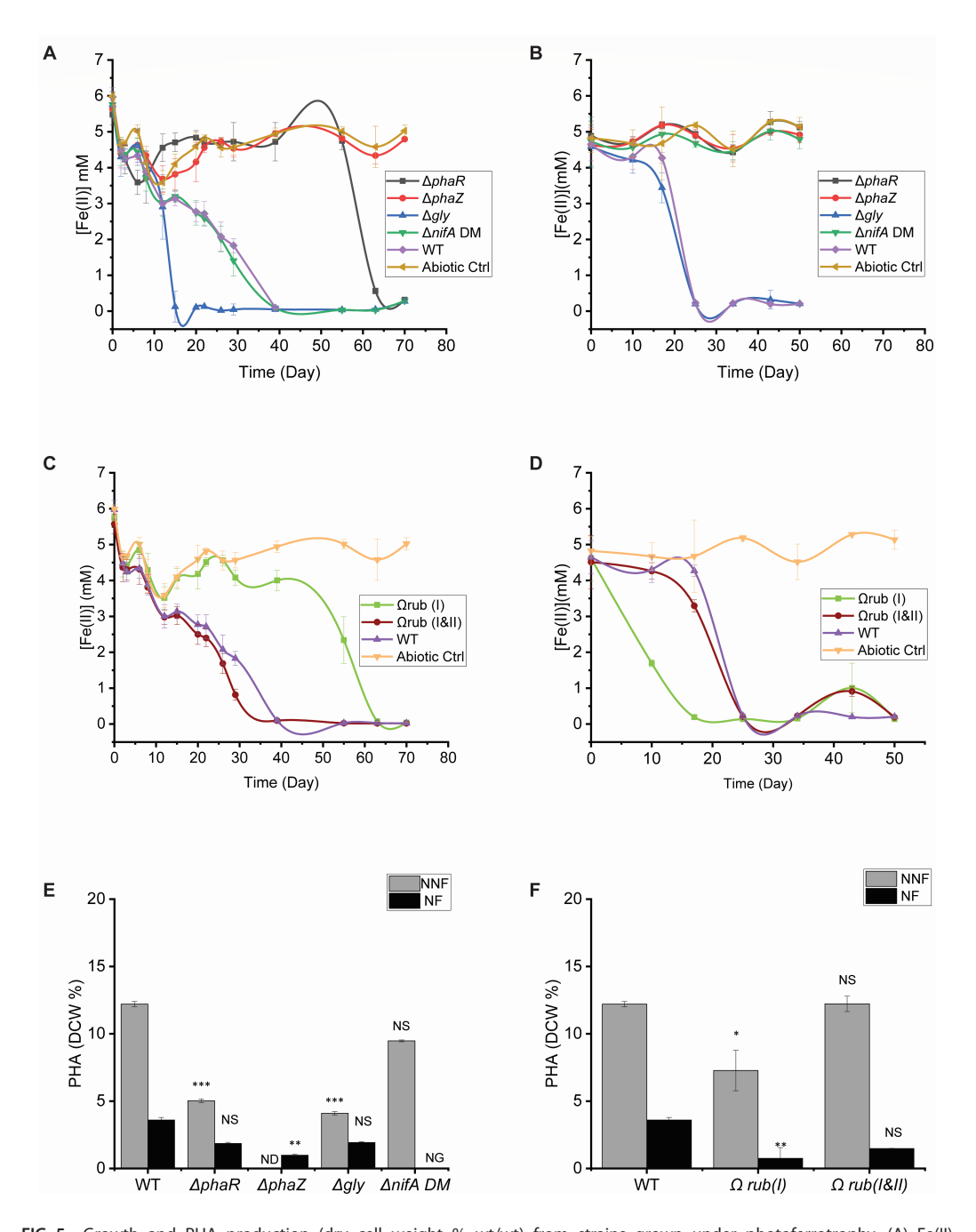


FIG 5 Growth and PHA production (dry cell weight % wt/wt) from strains grown under photoferrotrophy. (A) Fe(II) concentration variation from the mutants grown under non-nitrogen-fixing conditions. (B) Fe(II) concentration variation from the mutans during nitrogen-fixing conditions with N<sub>2</sub>. (C) Growth of the engineered RuBisCO strains under non-nitrogen-fixing conditions. (D) Growth of all the engineered RuBisCO stains under nitrogen-fixing growth conditions. (E) PHA productivity from mutants grown under non-nitrogen-fixing conditions photoferrotrophically. (F) PHA production from engineered RuBisCO strains grown under non-nitrogen-fixing or nitrogen-fixing conditions. Error bars from Fe(II) oxidation curves represent the standard deviation calculated from three replicates, while error bars from PHA production depict the standard error derived from biological triplicates. NFF, non-nitrogenfixing; NN, nitrogen fixing. The statistical differences in PHA production were calculated using two-tailed Student's test against the wild-type TIE-1. \* $P \le 0.05$ , \*\*P < 0.01, and \*\*\*P < 0.001; NS, not significant; ND, not detected; NG, no growth.

# Deletion of the various genes or overexpression of RuBisCO form I and II genes did not improve PHA production in TIE-1 under photoferrotrophy

To test PHA production obtained from growth during photoferrotrophy, samples were collected right after complete Fe(II) oxidation occurred. Lower PHA production (mg/L/cell and dry cell weight % wt/wt) was observed across all the mutants under growth with Fe(II) and non-nitrogen-fixing conditions compared to wild-type (Table 4; Fig. 5E). Among all the mutants, the  $\Delta nifA$  had the highest PHA production when grown under non-nitrogen-fixing conditions, with comparable levels to wild-type (P = 0.37).

 $\Delta phaR$  and  $\Delta gly$  showed the lowest production, about half that observed in wild-type when grown under non-nitrogen-fixing conditions (P=0). No PHA was detected from the  $\Delta phaZ$  mutant from the non-nitrogen-fixing conditions, which is linked to its inability to oxidize Fe(II). Like growth under non-nitrogen-fixing conditions, PHA productions from the  $\Delta phaR$ ,  $\Delta phaZ$ , and  $\Delta gly$  (P=0) strains during nitrogen-fixing conditions were overall lower than that obtained from wild-type (Fig. 5E and F). PHA production (mg/L/cell and dry cell weight % wt/wt) obtained from  $\Delta phaz$  under nitrogen-fixing conditions was ~3X (P=0.004) smaller than the wild-type (Table 4; Fig. 5E). No PHA was obtained from  $\Delta nifA$  when grown under nitrogen-fixing conditions because this strain is incapable of growth under such conditions.

A decrease in PHA production of about half was observed from the single engineered  $\Omega rub(l)$  strain under Fe(II) under non-nitrogen-fixing growth conditions (P=0.033) (Table 4; Fig. 5F). However, PHA production obtained from the  $\Omega rub(l\&l)$  was similar to the wild-type under growth with Fe(II) and non-nitrogen-fixing conditions (P=0.98). Like the trend obtained from the mutants, a decrease in PHA production was observed in the RuBisCO overexpressing strains under nitrogen-fixing conditions compared to the growth under non-nitrogen-fixing conditions. PHA production obtained from the  $\Omega rub(l)$  was  $\sim$ 4X (P=0.002) less than what was obtained from wild-type under nitrogen-fixing conditions.

# Growth under photoelectrotrophy under non-nitrogen-fixing conditions showed increased electron uptake from the engineered RuBisCO strains

In addition to its ability to grow autotrophically using hydrogen and Fe(II) as electron sources, TIE-1 can uptake electrons directly from poised electrodes (32). We grew the cells in bioelectrochemical reactors as described in Materials and Methods with freshwater media under nitrogen-fixing or non-nitrogen-fixing conditions. All mutant strains except  $\Delta phaR$  showed longer generation time compared to wild-type strains when grown under non-nitrogen-fixing conditions (Table 3) (P < 0.05).  $\Delta phaZ$  and  $\Delta gly$  exhibited significantly slower growth, as evidenced by a generation time ~4X longer than that of wild-type.  $\Delta nifA$  similarly exhibited an extended generation time, ~3X longer than that of wild-type (Table 3) (P = 0.0001).  $\Delta phaR$  did not exhibit a significant difference in its generation time compared to wild-type when grown under non-nitrogen-fixing conditions.  $\Omega rub(I)$  and  $\Omega rub(I&II)$  did not show a defect in generation time compared to wild-type under photoelectrotrophic non-nitrogen-fixing conditions.

We also measured the final OD of the strains at the end of the 14-day incubation. These values are reported as max OD in Table 3. The final OD values were ~1/2 lower than those of wild-type from  $\Delta phaZ$ ,  $\Delta gly$ , and  $\Delta nifA$  under non-nitrogen-fixing growth conditions (P < 0.05).  $\Delta phaR$  as well as the engineered strains  $\Omega rub(l)$  and  $\Omega rub(l&ll)$  had the same final OD as wild-type (Table 3) when grown under non-nitrogen-fixing conditions. Under photoelectrotrophic and nitrogen-fixing conditions, the generation time of  $\Delta phaR$ ,  $\Delta phaZ$ , as well as  $\Omega rub(l)$  and  $\Omega rub(l&ll)$  did not show any significant differences compared to wild-type (Table 1). The  $\Delta nifA$  did not show growth as expected. Due to the intricate nature of the experimental setup in photoelectrotrophic growth, we could only measure the cell density at initial and final times, preventing us from reporting lag time. We then assessed the ability of each constructed strain to capture electrons from a poised electrode. Under non-nitrogen-fixing conditions,  $\Delta phaR$ ,  $\Delta phaZ$ ,  $\Delta nifA$ , and  $\Omega rub(l)$  did not show a significant difference in current uptake when compared

to wild-type. However,  $\Delta gly$  showed ~6X (P = 0.001) lower current uptake, while  $\Omega rub(l\&ll)$  showed a decrease of ~2X (P = 0.009) in electron uptake when compared to wild-type (Fig. 6; Table 5).

Under nitrogen fixation conditions, electron uptake varied among strains. Notably,  $\Delta phaR$  exhibited an 18X reduction compared to wild-type (P=0.001). Additionally, both  $\Delta phaZ$  and  $\Delta gly$  displayed 4- and 2.6X lower uptake, respectively (P<0.001). The  $\Delta nifA$ , which expectedly was unable to grow under nitrogen fixation conditions, demonstrated an electron uptake like that of abiotic control. In contrast,  $\Omega rub(l)$  and  $\Omega rub(l\&l)$  displayed 4.5 and 16X higher electron uptake than wild-type, respectively (Table 5) (P<0.005).

# Overexpressing the RuBisCO form I and form II of TIE-1 increased its PHA production under photoelectrotrophic nitrogen-fixing growth conditions but not under non-nitrogen-fixing conditions

When grown under non-nitrogen-fixing conditions, PHA values obtained from the wild-type are sufficiently low so as to hinder us from comparing between strains (Table 4; Fig. 6E and F).

When grown under nitrogen-fixing conditions, we observed that the PHA production of phaR is similar to that of wild type. However, PHA production increased by 3X in  $\Delta phaZ$  and  $\Delta gly$  compared to wild-type (Table 4; Fig. 6E) (P < 0.05). PHA production by  $\Omega rub(l)$  and  $\Omega rub(l\&l)$  went 2X when compared to wild-type (P = 0.05). However, under nitrogen-fixing conditions, PHA produced from  $\Omega rub(l) = 0.24\%$  and  $\Omega rub(l\&l) = 0.16\%$  (dry cell weight % wt/wt) did not show statistically significant differences (P = 0.21) when evaluated against each other.

### DISCUSSION

In this study, we demonstrated that TIE-1 can be modified using genetic engineering and synthetic biology tools to enhance polyhydroxyalkanoate (PHA) production. We found that deleting the *phaR* regulator gene of PHA biosynthesis increased PHA production under non-nitrogen-fixing conditions with butyrate. Deletion of the glycogen synthase and the regulators of the nitrogen fixation pathways  $nifA_1$  and  $nifA_2$  increased PHA accumulation when grown under non-nitrogen-fixing conditions with hydrogen. More importantly, overexpressing RuBisCO form I and II using the  $\phi$ C31 integrase system in TIE-1 enhanced PHA production under photoheterotrophic growth with butyrate, regardless of the nitrogen source. This was also the case for autotrophic growth of these TIE-1 strains with hydrogen in non-nitrogen-fixing conditions. These results indicate that genetic engineering techniques, including our newly developed  $\phi$ C31 integration system, are effective for genetic manipulation in TIE-1 and increasing PHA production.

## Effect of deletions of genes in the PHA pathway on growth and PHA production in TIE-1

The specific regulatory role of PhaR (Rpal\_0531) has not been explored in TIE-1 before. Here, we discovered that deleting phaR did not significantly affect PHA production in TIE-1 across all growth conditions tested. However, the  $\Delta phaR$  mutant showed growth defects under non-nitrogen-fixing photoheterotrophic growth with butyrate and photoautotrophic growth with H<sub>2</sub> (Table S1; Table 3). Additionally, it exhibited decreased Fe(II) oxidation and electron uptake under nitrogen-fixing conditions compared to the wild-type (Fig. 5). In *Bradyrhizobium diazoefficiens* USDA110, inactivation of phaR decreased PHA accumulation and affected processes such as exopolysaccharide biosynthesis and heat stress tolerance (67). Our results suggest that PhaR's role in TIE-1 may extend to other pathways. Further transcriptomic and proteomic analyses of this mutant are needed to understand PhaR's broader regulatory roles.

We hypothesized that deleting the PHA depolymerase (PhaZ) in TIE-1 would inhibit PHA degradation, potentially increasing total PHA storage (Fig. 7). This expectation was based on findings from other purple nonsulfur bacteria, such as *Rhodobacter sphaeroides*, where the *phaZ* mutant showed improved PHA accumulation under nitrogen-rich

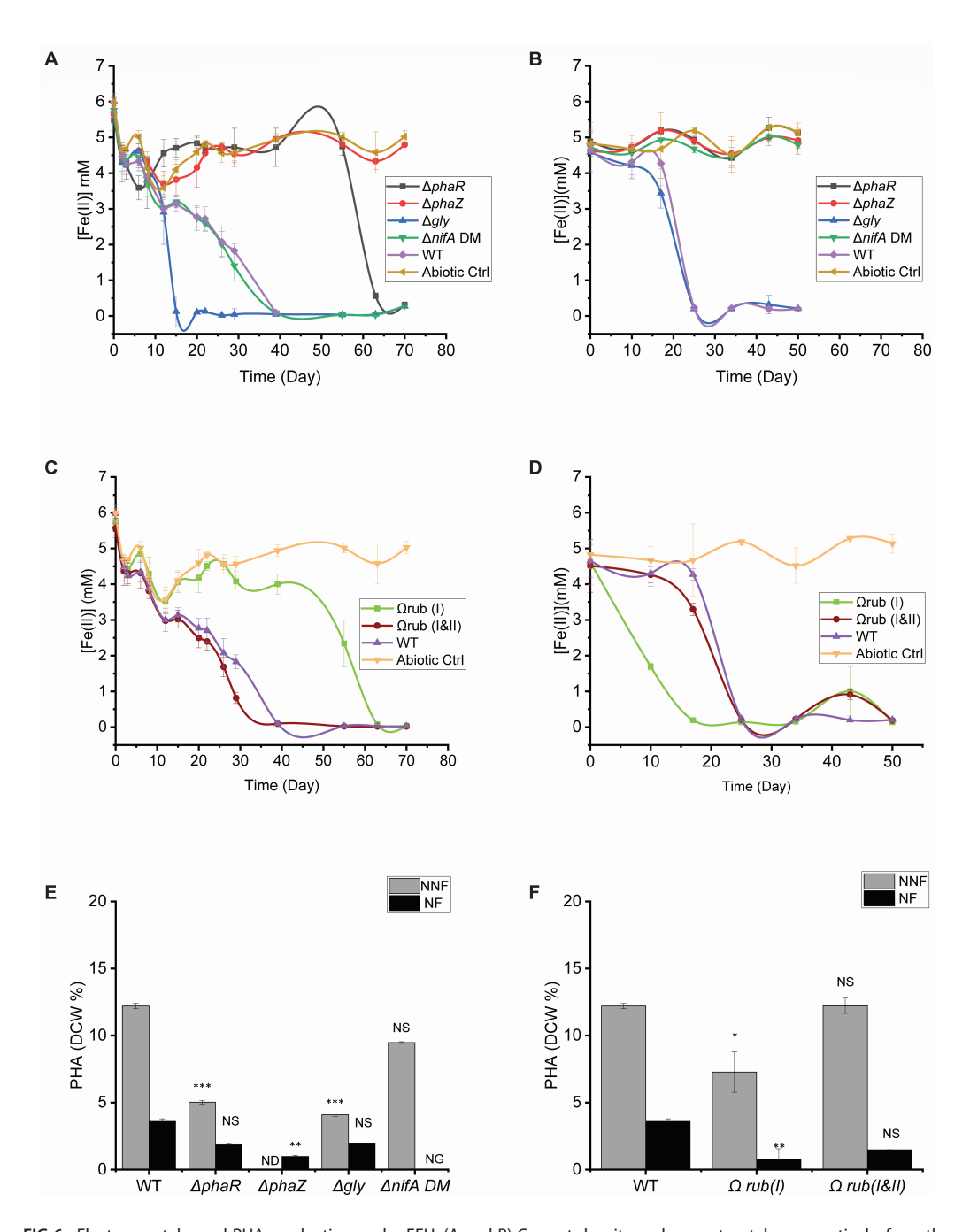


FIG 6 Electron uptake and PHA production under EEU. (A and B) Current density and current uptake, respectively, from the wild-type TIE-1 (WT) strain, the various mutants  $\Delta phaR$ ,  $\Delta phaZ$ ,  $\Delta gly$ , and  $\Delta nifA$  DM (double mutant), and the engineered strains  $\Omega rub(l)$  and  $\Omega rub(l\&l)$  under non-nitrogen-fixing growth conditions. (C and D) Current density and current uptake, respectively, from the wild-type TIE-1 (WT) strain, the various mutants  $\Delta phaR$ ,  $\Delta phaZ$ ,  $\Delta gly$ , and  $\Delta nifA$  DM (double mutant), and the engineered strains  $\Omega rub(l)$  and  $\Omega rub(l\&l)$  under nitrogen fixation conditions (N<sub>2</sub>). (E) PHA production (dry cell weight % wt/wt) from mutants grown under non-nitrogen-fixing and nitrogen-fixing conditions photoelectrotrophically. (F) PHA productivity from engineered RuBisCO strains grown under photoelectrotrophic non-nitrogen-fixing and nitrogen-fixing growth conditions. The statistical differences in PHA production were calculated using two-tailed Student's test against the wild-type TIE-1. \*P ≤ 0.05, \*\*P < 0.01, and \*\*\*P < 0.001 NNF, non-nitrogen fixing; NF, nitrogen fixing. Error bars represent standard errors from biological duplicates.

conditions (68). However, deleting phaZ did not significantly elevate PHA production in TIE-1. Unexpectedly, the absence of phaZ affected TIE-1's ability to oxidize Fe(II)

Downloaded from https://journals.asm.org/journal/aem on 01 July 2025 by 75.133.168.157.

**TABLE 5** Current uptake obtained from the different strains during photoelectroautotrophic growth under non-nitrogen-fixing or nitrogen-fixing conditions<sup>a</sup>

Strain	Current uptake (C)	
	Growth under non-nitrogen-fixing	Growth under nitrogen-fixing
	conditions	conditions
WT TIE-1	-0.7891 ± 0.02	-1.2359 ± 0.1027
$\Delta pha$ R	$-0.5257 \pm 0.2167 (P = 0.00018)$	$-0.0666 \pm 0.2182 (P = 0.0017)$
$\Delta phaZ$	$-0.6311 \pm 0.2118 (P = 0.0029)$	$-0.3019 \pm 0.1356 (P = 0.00092)$
Δgly	$-0.1241 \pm 0.0015 (P = 0.0001)$	$-0.4695 \pm 0.014 (P = 0.00036)$
ΔnifA	$-0.8461 \pm 0.0595 (P = 0.00026)$	$-0.0938 \pm 0.0356 (P = 0.00045)$
Ωrub(I)	$-0.9922 \pm 0.014 (P = 0.00177)$	$-5.6128 \pm 0.1182 (P = 0.00332)$
Ωrub(I &II)	$-0.3513 \pm 0.0283 \ (P = 0.0009)$	$-20.2604 \pm 0.2492 (P = 0.0008)$
Abiotic control	$-0.1159 \pm 0.067 (P = 0.00021)$	$-0.1474 \pm 0.0741 \ (P = 0.00067)$

 $<sup>^{</sup>a}$ Values are from two biological replicates,  $\pm$  standard deviation values.

during photoferrotrophic growth and decreased electron uptake under nitrogen-fixing photoelectrotrophic growth conditions. These findings suggest that disrupting PHA depolymerase alters the electron balance within TIE-1, meriting further bioinformatics and proteomics studies.

# Effects of deletion of a potential competitive pathway on PHA production in TIE-1

We hypothesized that deleting the glycogen synthase (gly) gene would prevent glucose accumulation as glycogen, allowing glucose to be converted into pyruvate via glycolysis and subsequently into acetyl-CoA by pyruvate dehydrogenase, as illustrated in Fig. 7. Increased availability of acetyl-CoA could enhance PHA production. Contrary to our expectations, deletion of the glycogen synthase gene increased PHA production only under non-nitrogen-fixing conditions with hydrogen. A decrease in PHA production was observed under photoheterotrophic growth with butyrate and photoautotrophic growth with Fe(II) under nitrogen-fixing growth conditions. Additionally, a shorter generation time under non-nitrogen-fixing conditions with butyrate and Fe(II) suggests that blocking glycogen accumulation might channel carbon into biomass production rather than PHA production. Similar findings were reported in *Synechocystis sp.* PCC 6803, where glycogen was hypothesized to serve as a carbon source for PHA synthesis under nitrogen starvation conditions (58). Although autotrophic growth with hydrogen could be considered stressful compared to photoheterotrophic growth, the  $\Delta gly$  strain seems to prioritize biomass increase over PHA production under these conditions.

### Effect of nitrogen fixation and nifA gene deletion on PHA production in TIE-1

Nitrogen fixation has been reported to increase PHA production (27, 41, 61). We observed this trend under photoheterotrophic growth with butyrate and photoautotrophic growth with hydrogen across most strains. However, under photoautotrophic growth with Fe(II), PHA production decreased under nitrogen-fixing compared to non-nitrogen-fixing conditions, with similar values obtained from photoelectrotrophic conditions under the two nitrogen sources. These observations align with those of our previous studies (27). The distinct responses under different growth conditions suggest potential variation in the regulatory mechanisms employed by TIE-1 under nitrogen fixation conditions.

Nitrogen fixation requires substantial reducing power (37). We investigated the impact of deleting two key activators of the nitrogenase genes,  $nifA_1$  and  $nifA_2$ , to redirect NADPH toward PHA biosynthesis (Fig. 7). Contrary to our expectation, deleting nifA genes mainly decreased PHA production. However, under non-nitrogen-fixing photoheterotrophic growth with 10 mM butyrate, this strain showed a decreased generation time by approximately 25% (P = 0.007, Table 1; Table S2) suggesting that

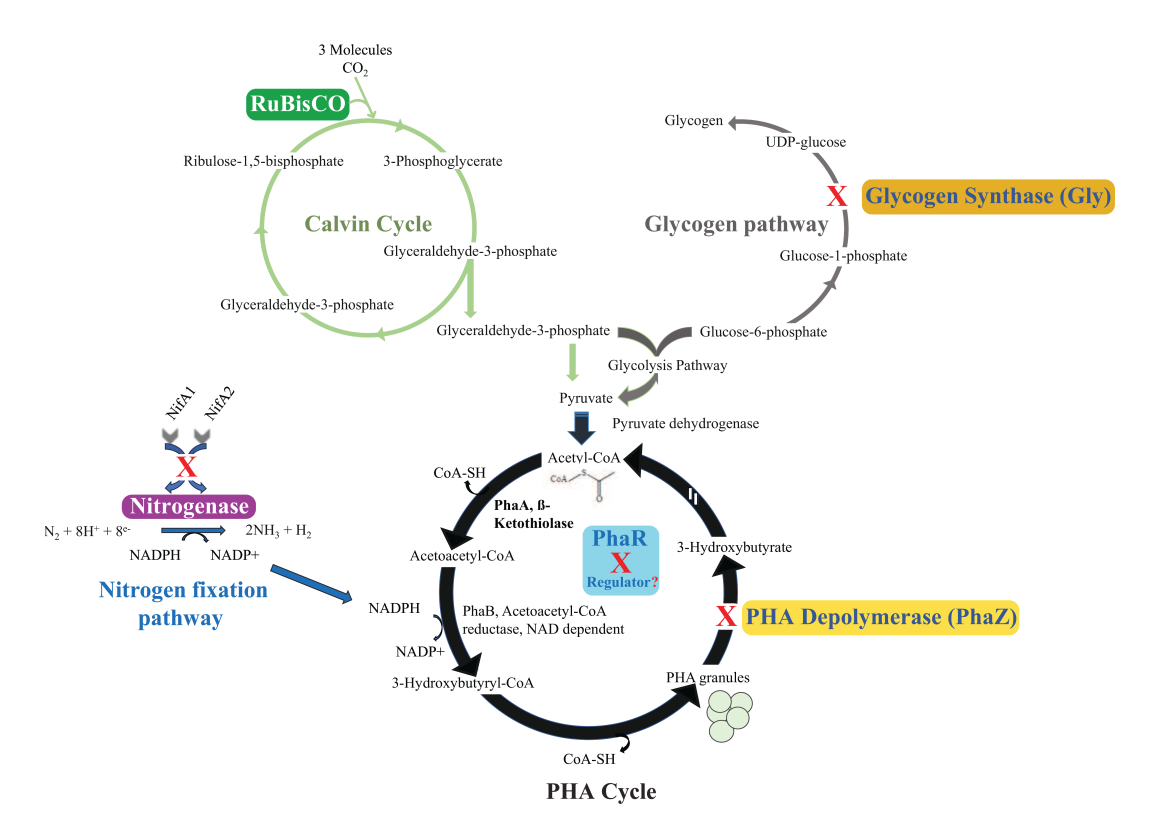


FIG 7 Summary of pathways targeted to increase PHA production in TIE-1. (A) Calvin–Benson–Bassham cycle: overexpression of RuBisCo forms I and II. (B) Nitrogen fixation pathway: deletion of the two regulators *nifA1* and *nifA2* gene. (C) Glycogen pathway: deletion of the glycogen synthase gene. (D) PHA biosynthesis pathway: deletion of the PHA depolymerease *phaZ* and the regulator *phaR* genes. Red X represents deletion.

it favored growth over PHA production. Due to the highly reduced nature of butyrate and the presence of sodium bicarbonate in our media, it is possible that the electrons intended for nitrogen fixation were instead diverted to  $CO_2$  fixation for redox balance. This diversion could have contributed to biomass production rather than PHA synthesis. It is worth mentioning though that like the increase in n-butanol production observed in  $\Delta nifA$  (37), we noticed an increase in PHA production from this strain grown under non-nitrogen-fixing photoautotrophic conditions with hydrogen (37).

### Effect of overexpressing RuBisCO genes on PHA production in TIE-1

By increasing  $CO_2$  fixation through the Calvin–Benson–Bassham, we aim to increase acetyl–CoA abundance, leading to higher PHA production as shown in Fig. 7. Similar observations were reported in *Ralstonia eutropha*, where expressing a heterologous cyanobacterial RuBisCO gene resulted in a significant 99.7% increase in PHA accumulation under autotrophic growth. In TIE-1, overexpression of RuBisCO form I led to a  $\sim 2X$  increase in PHA production under both non-nitrogen- and nitrogen-fixing conditions. Overexpression of both RuBisCO forms I and II resulted in a  $\sim 5X$  increase under photoheterotrophic growth with butyrate and a  $\sim 3X$  increase under nitrogen-fixing conditions. The combined overexpression of both forms had a cumulative effect on PHA production. Surprisingly, overexpression of RuBisCO form I alone showed a growth defect under photoheterotrophy with butyrate and impaired Fe(II) oxidation under non-nitrogen-fixing conditions. This defect disappeared when both RuBisCO forms were overexpressed, suggesting a compensatory effect.

### **Future directions**

We conclude that overexpressing RuBisCO form I and II increased PHA production in TIE-1 more efficiently than deleting competitive pathways. These ( $\Omega rubI$ ) and  $\Omega rub(I\&II)$  engineered strains could be envisioned as potential candidates for PHA production in larger scale, both under heterotrophic and autotrophic growth conditions. Larger reactors like those developed for biodiesel production by Awogbemi *et al.* (69) could be envisioned for these purposes. Using the  $\phi$ C31 system, it would be highly valuable to investigate the effect of overexpressing other genes that could potentially enhance PHA production in TIE-1. Given that the deletion of *phaR*, glycogen synthase (*gly*), and *nifA* genes did not result in a consistent increase in PHA production, it would be intriguing to initiate overexpression experiments with each of these genes. Additionally, gene overexpression could be extended to the PHA polymerase (*phaC*) gene using the integration system developed in this study to further boost PHA production in TIE-1.

Furthermore, it would be beneficial to assess the effects of creating combinatorial strains by overexpressing *phaR*, *phaZ*, glycogen synthase, and the *nifA* regulator genes, alongside the simultaneous overexpression of both native and non-native RuBisCO form I and II genes in TIE-1. This combinatorial approach may provide deeper insights into the regulatory networks and metabolic pathways influencing PHA synthesis in this organism. We also suggest that metabolic flux balance analysis and other machine learning methods might help us determine optimal mutant and overexpression strain construction for maximizing PHA production.

### **MATERIALS AND METHODS**

### Bacterial strains, media, and growth conditions

Table 1 lists all the strains used in the study. Lysogeny broth (LB) was used for growth of all *E. coli* strains at 37°C. *Rhodopseudomonas palustris* TIE-1 was grown in the medium containing 3 g/L yeast extract, 3 g/L peptone, 10 mM MOPS [3 N (morpholino) propane-sulfonic acid] (pH 7.0), and 10 mM succinate (YPSMOPS) at 30°C. LB and YPSMOPS agar plates were prepared with the addition of 15 g/L agar. When needed, an antibiotic or sucrose was added as indicated in Table S3. All *E. coli* strains were grown on lysogeny broth (LB) at 37°C. Table 1 contains a list of the strains used in the study. Table S3 shows the concentration of antibiotics used as positive and negative selection components.

Anerobic growth of TIE-1 with hydrogen, Fe(II), or using poised electrodes was performed as previously described (27). Because transitioning between heterotrophic and photoautotrophic growth conditions in  $H_2$  and Fe(II) requires a metabolic shift in TIE-1 (27), to obtain stable growth, cells were first pre-grown in the yeast extract and then transferred into freshwater basal medium with  $H_2$  for an additional pre-growth before the growth study (27). For growth under photoelectrotrophy, the cells were grown with YP, washed three times with freshwater media, and used directly to innoculate the reactors to reduce contamination. The bioelectrochemical systems were set up as previously described (27) with the electrode modified to carbon felt (dimension 1 × 1×.5 cm).

### **Plasmid construction**

All the plasmids used in this study are listed in Table 2. The kanamycin and chloramphenicol gene sequences were PCR-amplified from pSRKKm and pSRKCm, respectively. All these antibiotic resistance marker genes were then cloned into the pJQ200KS plasmid separately to replace the gentamicin resistance gene, resulting in pWB091 and pWB092. All the primers used are listed in Table S4.

### Construction of engineered TIE-1 overexpressing RuBisCO form I and form II

Strains were constructed as described previously using markerless integration (34). pWB107 and pWB108 were individually conjugated into TIE-1 through *E. coli* S17-1/ $\lambda$ .

After two successive homologous recombination processes, successful integrants were screened by the PCR, as shown in Fig. S4 and S5.

### **TIE-1 electroporation**

To prepare electrocompetent cells, the TIE-1 strain was inoculated in 500 mL YPSMOPS and then incubated at 30°C. After reaching an OD<sub>660</sub> of 0.5–0.6, the culture was centrifuged and washed at 4°C at 4,000 X g for 10 minutes. After washing five times with 10% glycerol, the cell pellet was resuspended in 2 mL of ice-cold 10% glycerol. This resuspension was aliquoted by 50  $\mu$ L per sample and then saved in -80°C. For every electroporation, 0.2  $\mu$ g of plasmid was added to 50  $\mu$ L thawed electrocompetent cells and mixed well. This mixture was added to 1-mm gap electroporation cuvettes, and then cells were electroporated at 1.8 kV using a Biorad gene Micropulser. After electroporation, the mixture was added to 2 mL warmed Super Optimal Broth (SOB) or LB and grown for 45 minutes. Ten microliters, 100  $\mu$ L, 500  $\mu$ L, and the remainder of the culture were plated on the selective medium. Because these plates were further imaged by Nikon A1, glass Petri dishes were used instead of plastic Petri dishes.

### Imaging of mCherry

After 4 to 5 days of incubation, the plated electroporated cultures expressing *mCherry* were imaged using the Nikon A1 confocal Eclipse Ti2 Microscope. For each plate, an image of the whole plate was captured using a camera through both the brightfield and the Texas-red channel (excitation 586 nm; emission 603 nm) with a 10X objective. The colony number of each plate was quantified using NIS-Elements AR Analysis 5.11.01 64-bit software.

# Calculations of transformation efficiency and colony-forming unit per optical density

We evaluated our  $\phi$ C31 phage integration systems by calculating the transformation efficiency as calculated by the following equation:

$$Transformation efficiency = \frac{Colony number post-electroporation}{amount of plasmid (\mu g)}$$

The editing efficiency is calculated by:

$$Editing \ efficiency = \ \frac{Number \ of \ engineered \ colonies}{Number \ of \ initial \ colonies}$$

### **Construction of TIE-1 mutants**

The following strains were constructed using the markerless deletion method, as illustrated in Fig. S1: phaZ mutant  $\Delta Rpal\_0578$ , and phaR mutant ( $\Delta rpal\_0531$ ). The two mutants  $\Delta gly$  and the  $\Delta nifA$  double mutant have been described previously (37). The mutant constructions were as follows: 1 kb upstream and 1 kb downstream of each of the genes of interest were PCR-amplified and cloned into the cloning vector pJQ200KS. The constructed plasmids were then electroporated into the donor strain E.coli S17-1/ $\lambda$ . The E.coli donor strains carrying the constructed plasmids were conjugated with the TIE-1 wild-type. After two consecutive homologous recombination events, successful mutant candidates were screened using the PCR (Fig. S2) and the primers listed in Table S5.

### PHA extraction and analysis

PHA samples were extracted from 5 mL of the liquid bacterial culture, and the organic phases were analyzed using LC-MS using a method we developed as previously reported

(27). About 325  $\mu$ L of methanol, 400  $\mu$ L chloroform, and 75  $\mu$ L of sulfuric acid were simultaneously added to the sample pellet. The mixtures were incubated at 95°C for only 1 hour to minimize the potential loss of methylated products in the aqueous phase. Subsequently, phase separation and acid elimination were performed by the addition of 500  $\mu$ L of LC-MS-grade water. The organic phases were dried using a speed vacuum. Dried crotonic acid was then resuspended in 50% acetonitrile/50% water and analyzed using an Agilent Technologies 6420 Triple Quad LC/MS. Crotonic acid was detected with a mass-to-charge ratio (m/z) of 87. Standard curves of 1, 10, 50, and 100 ppm concentrations were created from a polyhydroxybutyrate (PHB) standard purchased from Sigma Aldrich. Standards were prepared the same way as the samples and were used for the determination of PHA from different samples.

PHA (mg/L) concentrations were determined using the standard curve generated from the counts obtained from the following dry powder PHB concentrations: 1, 10, 50, and 100 ppm.

PHA (mg/L/Cell) was obtained from the following equation:

$$PHA (mg/L/ Cell) = \frac{PHA (mg/L)}{Cell number}$$

PHA productivity in (mg/L/cell/hour) was obtained from the following equation:

PHA productivity = 
$$\frac{\frac{PHA}{\text{cell number}}}{\text{growth time}}$$

### OD measurements, cell counts, and cell volume determinations

OD measurements were performed using a Spectronic 200 (Thermo Fisher Scientifc, USA) at 660 nm. Cell enumerations were performed and have been used previously to report PHA production (27, 70). The cell volume was determined by staining TIE-1 with FM 1-43FX membrane stain and visualized under a Nikon, A1 confocal microscope Model Eclipse Ti2. Stained cells were 3-D-imaged using the FM 1-43 laser channel at 471 nm. Cells were stained according to the manufacturer's recommendations with a slight modification. Briefly, 1 mL of the culture cell of  $OD_{660}$  ~1 was spun down at 15 k rpm for 1 minute, washed once with 1X PBS, and resuspended in 100 µL of ice-cold methanol for 2 minutes. An additional washing with 100 μL ice-cold acetone was performed. Cells were finally resuspended in 1.5 mL 1X PBS buffer and stained with the FM-1-43FX dye for 10 minutes in the dark. Cells were mounted on a coverslip coated with 10% poly-L-lysine and air-dried before observation under the microscope. The TIE-1 volume was determined as 1.048 pm³ using ~1,000 individual cells. PHA cell % vol/vol was obtained by dividing the volume of PHA per cell with the cell volume assuming that PHA density is 1.22 g/cm<sup>3</sup> (71), and the cell % wt/wt fresh weight was obtained by dividing PHA mass by the fresh cell mass assuming that the cell density is 1.1 g/cm<sup>3</sup> (72). The dry cell weight was estimated to be 40% of the fresh cell weight (73).

# Genomic DNA sequencing of the engineered RuBisCo strains $\Omega rub(l)$ and $\Omega rub(l\&ll)$

DNA extracted from each strain was submitted to Plasmidsaurus. Bacterial genome sequencing was performed by Plasmidsaurus using Oxford Nanopore Technology. Raw reads were downloaded from Plasmidsaurus and were analyzed and annotated on KBase (74) using the following pipeline.

Read quality filtering was performed using Filtlong (75), keeping the best 90% of reads by quality score, with a minimum length of 1,000 bp. Quality control of filtered reads was performed using FastQC (76). Assembly of reads was performed using the long-read assemblers MiniASM (77) and Flye (78). Quality of assemblies was checked using Quast (79). Finished assemblies were annotated for features (e.g., genes and

RNA-coding regions) using RAST (80). Genomes were uploaded to the RAST server (81) viewed using the SEED viewer (82), and construct integration sites were confirmed using BLAST (83).

### **ACKNOWLEDGMENTS**

We would like to thank Dr. Joshua Blodgett for facilitating PHA analysis using LC-MS. We would like to thank Jungwoo Lee for proofreading the manuscript.

This work was supported by the following grants to A.B.: The David and Lucile Packard Foundation Fellowship (201563111), the U.S. Department of Energy (grant number DESC0014613), and the U.S. Department of Defense, Army Research Office (grant number W911NF-18-1-0037), Gordon and Betty Moore Foundation, National Science Foundation (Grant Number 2021822, Grant Number 2124088, Grant Number 2117198, and Grant Number 2300081), the U.S. Department of Energy by Lawrence Livermore National Laboratory under Contract DEAC5207NA27344 (LLNL-JRNL-812309), NIGMS grant (NIHR01GM141344), and a DEPSCOR grant (FA9550-21-1-0211). A.B. was also funded by a Collaboration Initiation Grant, an Office of the Vice-Chancellor of Research Grant, an International Center for Energy, Environment, and Sustainability Grant, and a SPEED grant from Washington University in St. Louis.

T.O.R., W.B., M.S., J.O., H.S., and E.C. performed all the experiments. R.K. assisted with the bioelectrochemical experiments. BG assisted with the genome assembly. T.O.R., W.B., and A.B. wrote the manuscript with input from all authors.

### **AUTHOR AFFILIATIONS**

<sup>1</sup>Department of Biology, Washington University in St. Louis, St. Louis, Missouri, USA <sup>2</sup>LifeFoundry, San Jose, California, USA

### **AUTHOR ORCIDs**

Tahina Onina Ranaivoarisoa http://orcid.org/0009-0005-4110-8960
Rengasamy Karthikeyan http://orcid.org/0009-0002-5486-2653
Eric Conners http://orcid.org/0000-0002-0664-307X
Brian Gallagher http://orcid.org/0000-0002-7707-1371
Arpita Bose http://orcid.org/0000-0002-7526-0988

### **FUNDING**

Funder	Grant(s)	Author(s)
David and Lucile Packard	201563111	Tahina Onina Ranaivoarisoa
Foundation (PF)		Wei Bai
		Rengasamy Karthikeyan
		Hope Steele
		Eric Conners
		Arpita Bose
U.S. Department of Energy (DOE)	DESC0014613	Tahina Onina Ranaivoarisoa
		Wei Bai
		Rengasamy Karthikeyan
		Arpita Bose
DOD   USA   AFC   CCDC   Army	W911NF-18-1-0037	Tahina Onina Ranaivoarisoa
Research Office (ARO)		Wei Bai
		Rengasamy Karthikeyan
		Arpita Bose

Funder	Grant(s)	Author(s)
Gordon and Betty Moore Foundation (GBMF)		Arpita Bose
National Science Foundation	2021822, 2124088,	Tahina Onina Ranaivoarisoa
(NSF)	2117198, 2300081	Wei Bai
		Rengasamy Karthikeyan
		Hope Steele
		Miriam Silberman
		Jennifer Olabode
		Eric Conners
		Brian Gallagher
DOE   NNSA   Lawrence	LLNL-JRNL-812309	Tahina Onina Ranaivoarisoa
Livermore National Laboratory (LLNL)		Rengasamy Karthikeyan
(LLIVL)		Arpita Bose
HHS   NIH   National Institute	NIHR01GM141344	Tahina Onina Ranaivoarisoa
of General Medical Sciences (NIGMS)		Rengasamy Karthikeyan
(INIGINIS)		Arpita Bose

### **AUTHOR CONTRIBUTIONS**

Tahina Onina Ranaivoarisoa, Conceptualization, Data curation, Formal analysis, Investigation, Methodology, Project administration, Resources, Software, Supervision, Validation, Visualization, Writing – original draft, Writing – review and editing | Wei Bai, Conceptualization, Data curation, Formal analysis, Investigation, Methodology, Resources, Supervision, Validation, Visualization, Writing – original draft, Writing – review and editing | Rengasamy Karthikeyan, Data curation, Formal analysis, Investigation, Methodology, Resources, Validation, Visualization, Writing – review and editing | Hope Steele, Data curation, Investigation, Methodology | Miriam Silberman, Data curation, Investigation | Jennifer Olabode, Data curation | Eric Conners, Data curation, Methodology, Validation, Writing – review and editing | Brian Gallagher, Data curation, Data curation, Formal analysis, Funding acquisition, Investigation, Methodology, Project administration, Resources, Software, Supervision, Validation, Visualization, Writing – original draft, Writing – review and editing

### **DIRECT CONTRIBUTION**

This article is a direct contribution from Arpita Bose, a member of the *Applied and Environmental Microbiology* Editorial Board, who arranged for and secured reviews by Baptiste Leroy, Universite de Mons, and Daniel Puyol, Universidad Rey Juan Carlos.

### **DATA AVAILABILITY**

All data in the paper will be provided by authors upon request.

### **ADDITIONAL FILES**

The following material is available online.

### Supplemental Material

**Supplemental material (AEM01438-24-s0001.docx).** Figures S1 to S5; Tables S1 to S5.

### **REFERENCES**

- Keasling JD. 2010. Manufacturing molecules through metabolic engineering. Science 330:1355–1358. https://doi.org/10.1126/science. 1193990
- Müller T, Schick S, Beck J, Sprenger G, Takors R. 2023. Synthetic mutualism in engineered *E. coli* mutant strains as functional basis for microbial production consortia. Eng Life Sci 23. https://doi.org/10.1002/ elsc 202100158
- Panda S, Zhou K. 2023. Engineering microbes to overproduce natural products as agrochemicals. Synth Syst Biotechnol 8:79–85. https://doi. org/10.1016/j.synbio.2022.11.005
- 4. Kyriakou M, Patsalou M, Xiaris N, Tsevis A, Koutsokeras L, Constantinides G, Koutinas M. 2020. Enhancing bioproduction and thermotolerance in *Saccharomyces cerevisiae* via cell immobilization on biochar: application in a citrus peel waste biorefinery. Renewable Energy.
- Saini M, Hong Chen M, Chiang C-J, Chao Y-P. 2015. Potential production platform of n-butanol in *Escherichia coli*. Metab Eng 27:76–82. https://doi.org/10.1016/j.ymben.2014.11.001
- Wang J, Lu X, Ying H, Ma W, Xu S, Wang X, Chen K, Ouyang P. 2018. A novel process for cadaverine bio-production using A consortium of two engineered *Escherichia coli*. Front Microbiol 9:1312. https://doi.org/10. 3389/fmicb.2018.01312
- Li H, Gao S, Zhang S, Zeng W, Zhou J. 2021. Effects of metabolic pathway gene copy numbers on the biosynthesis of (2S)-naringenin in Saccharomyces cerevisiae. J Biotechnol 325:119–127. https://doi.org/10. 1016/j.jbiotec.2020.11.009
- Orozco PA. 2023. Lanthipeptide biosynthesis in marine Synechococcus: expression, characterization, and bioengineering of a wide variety of synechococsins. https://research.rug.nl/en/publications/lanthipeptidebiosynthesis-in-marine-synechococcus-expression-cha.
- Zhang F, Rodriguez S, Keasling JD. 2011. Metabolic engineering of microbial pathways for advanced biofuels production. Curr Opin Biotechnol 22:775–783. https://doi.org/10.1016/j.copbio.2011.04.024
- Miller EM, Nickoloff JA. 1995. Escherichia coli electrotransformation, p 105–113. In Electroporation protocols for microorganisms. Springer.
- Mäkelä J, Sherratt DJ. 2020. Organization of the Escherichia coli chromosome by a MukBEF axial core. Mol Cell 78:250–260. https://doi. org/10.1016/j.molcel.2020.02.003
- van Rossum HM, Kozak BU, Pronk JT, van Maris AJA. 2016. Engineering cytosolic acetyl-coenzyme A supply in Saccharomyces cerevisiae: pathway stoichiometry, free-energy conservation and redox-cofactor balancing. Metab Eng 36:99–115. https://doi.org/10.1016/j.ymben.2016. 03.006
- DiCarlo JE, Norville JE, Mali P, Rios X, Aach J, Church GM. 2013. Genome engineering in Saccharomyces cerevisiae using CRISPR-Cas systems. Nucleic Acids Res 41:4336–4343. https://doi.org/10.1093/nar/gkt135
- Cakar ZP, Turanli-Yildiz B, Alkim C, Yilmaz U. 2012. Evolutionary engineering of Saccharomyces cerevisiae for improved industrially important properties. FEMS Yeast Res 12:171–182. https://doi.org/10. 1111/j.1567-1364.2011.00775.x
- den Haan R, Kroukamp H, Mert M, Bloom M, Görgens JF, van Zyl WH. 2013. Engineering Saccharomyces cerevisiae for next generation ethanol production. J Chem Techn Biotech 88:983–991. https://doi.org/10.1002/ jctb.4068
- Abbott DA, Zelle RM, Pronk JT, van Maris AJA. 2009. Metabolic engineering of Saccharomyces cerevisiae for production of carboxylic acids: current status and challenges. FEMS Yeast Res 9:1123–1136. https://doi.org/10.1111/j.1567-1364.2009.00537.x
- Cao X, Yu W, Chen Y, Yang S, Zhao ZK, Nielsen J, Luan H, Zhou YJ. 2023. Engineering yeast for high-level production of diterpenoid sclareol. Metab Eng 75:19–28. https://doi.org/10.1016/j.ymben.2022.11.002
- Parapouli M, Vasileiadis A, Afendra A-S, Hatziloukas E. 2020. Saccharomyces cerevisiae and its industrial applications. AIMS Microbiol 6:1–31. https://doi.org/10.3934/microbiol.2020001
- Luo H, Zheng P, Bilal M, Xie F, Zeng Q, Zhu C, Yang R, Wang Z. 2020. Efficient bio-butanol production from lignocellulosic waste by elucidating the mechanisms of *Clostridium acetobutylicum* response to phenolic inhibitors. Sci Total Environ 710:136399. https://doi.org/10. 1016/j.scitotenv.2019.136399

- Wang Q, Yu H, Xia Y, Kang Z, Qi Q. 2009. Complete PHB mobilization in *Escherichia coli* enhances the stress tolerance: a potential biotechnological application. Microb Cell Fact 8:1–9. https://doi.org/10.1186/1475-2859-8-47
- Ferreira S, Pereira R, Wahl SA, Rocha I. 2020. Metabolic engineering strategies for butanol production in *Escherichia coli*. Biotechnol Bioeng 117:2571–2587. https://doi.org/10.1002/bit.27377
- Gong C, Cao L, Fang D, Zhang J, Kumar Awasthi M, Xue D. 2022. Genetic manipulation strategies for ethanol production from bioconversion of lignocellulose waste. Bioresour Technol 352:127105. https://doi.org/10. 1016/j.biortech.2022.127105
- Calero P, Nikel Pl. 2019. Chasing bacterial chassis for metabolic engineering: a perspective review from classical to non-traditional microorganisms. Microb Biotechnol 12:98–124. https://doi.org/10.1111/ 1751-7915.13292
- Brown B, Wilkins M, Saha R. 2022. Rhodopseudomonas palustris: a biotechnology chassis. Biotechnol Adv 60:108001. https://doi.org/10. 1016/j.biotechadv.2022.108001
- Azambuja SPH, Goldbeck R. 2020. Butanol production by Saccharomyces cerevisiae: perspectives, strategies and challenges. World J Microbiol Biotechnol 36:48. https://doi.org/10.1007/s11274-020-02828-z
- Jiao Y, Kappler A, Croal LR, Newman DK. 2005. Isolation and characterization of a genetically tractable photoautotrophic Fe(II)-oxidizing bacterium, *Rhodopseudomonas palustris* strain TIE-1. Appl Environ Microbiol 71:4487–4496. https://doi.org/10.1128/AEM.71.8.4487-4496.
- Ranaivoarisoa TO, Singh R, Rengasamy K, Guzman MS, Bose A. 2019. Towards sustainable bioplastic production using the photoautotrophic bacterium *Rhodopseudomonas palustris* TIE-1. J Ind Microbiol Biotechnol 46:1401–1417. https://doi.org/10.1007/s10295-019-02165-7
- Karthikeyan R, Singh R, Bose A. 2019. Microbial electron uptake in microbial electrosynthesis: a mini-review. J Ind Microbiol Biotechnol 46:1419–1426. https://doi.org/10.1007/s10295-019-02166-6
- Cabecas Segura P, Onderwater R, Deutschbauer A, Dewasme L, Wattiez R, Leroy B. 2022. Study of the production of poly(Hydroxybutyrate-co-hydroxyhexanoate) and Poly(Hydroxybutyrate-co-Hydroxyvalerate-co-Hydroxyhexanoate) in *Rhodospirillum rubrum*. Appl Environ Microbiol 88:e0158621. https://doi.org/10.1128/AEM.01586-21
- Bayon-Vicente G, Zarbo S, Deutschbauer A, Wattiez R, Leroy B. 2020. Photoheterotrophic assimilation of valerate and associated polyhydrox-yalkanoate production by *Rhodospirillum rubrum* Appl Environ Microbiol 86:e00901-20. https://doi.org/10.1128/AEM.00901-20
- Conners E, Rengasamy K, Ranaivoarisoa T, Bose A. 2024. The phototrophic purple non-sulfur bacteria *Rhodomicrobium* spp. are novel chassis for bioplastic production. Microb Biotechnol. https://doi.org/10.1111/ 1751-7915.14552.
- Bose A, Gardel EJ, Vidoudez C, Parra EA, Girguis PR. 2014. Electron uptake by iron-oxidizing phototrophic bacteria. Nat Commun 5:3391. https://doi.org/10.1038/ncomms4391
- Rengasamy K, Ranaivoarisoa T, Singh R, Bose A. 2018. An insoluble iron complex coated cathode enhances direct electron uptake by Rhodopseudomonas palustris TIE-1. Bioelectrochemistry 122:164–173. https://doi.org/10.1016/j.bioelechem.2018.03.015
- Bose A, Newman DK. 2011. Regulation of the phototrophic iron oxidation (pio) genes in *Rhodopseudomonas palustris* TIE-1 is mediated by the global regulator, FixK. Mol Microbiol 79:63–75. https://doi.org/10. 1111/j.1365-2958.2010.07430.x
- Rengasamy K, Ranaivoarisoa T, Bai W, Bose A. 2021. Magnetite nanoparticle anchored graphene cathode enhances microbial electrosynthesis of polyhydroxybutyrate by *Rhodopseudomonas palustris* TIE-1. Nanotechnology 32:035103. https://doi.org/10.1088/1361-6528/ abbe58
- Rabaey K, Girguis P, Nielsen LK. 2011. Metabolic and practical considerations on microbial electrosynthesis. Curr Opin Biotechnol 22:371–377. https://doi.org/10.1016/j.copbio.2011.01.010
- Bai W, Ranaivoarisoa TO, Singh R, Rengasamy K, Bose A. 2021. N-butanol production by *Rhodopseudomonas palustris* TIE-1. Commun Biol 4:1257. https://doi.org/10.1038/s42003-021-02781-z

- Gupta D, Sutherland MC, Rengasamy K, Meacham JM, Kranz RG, Bose A.
   2019. Photoferrotrophs produce a PioAB electron conduit for extracellular electron uptake. MBio 10. https://doi.org/10.1128/mBio.02668-19
- Singh R, Ranaivoarisoa TO, Gupta D, Bai W, Bose A. 2020. Genetic redundancy in iron and manganese transport in the metabolically versatile bacterium *Rhodopseudomonas palustris* TIE-1. Appl Environ Microbiol 86:e01057-20. https://doi.org/10.1128/AEM.01057-20
- Guzman MS, Rengasamy K, Binkley MM, Jones C, Ranaivoarisoa TO, Singh R, Fike DA, Meacham JM, Bose A. 2019. Phototrophic extracellular electron uptake is linked to carbon dioxide fixation in the bacterium Rhodopseudomonas palustris. Nat Commun 10:1355. https://doi.org/10. 1038/s41467-019-09377-6
- McKinlay JB, Oda Y, Rühl M, Posto AL, Sauer U, Harwood CS. 2014. Nongrowing *Rhodopseudomonas palustris* increases the hydrogen gas yield from acetate by shifting from the glyoxylate shunt to the tricarboxylic acid cycle. J Biol Chem 289:1960–1970. https://doi.org/10.1074/jbc. M113.527515
- Gosse JL, Engel BJ, Rey FE, Harwood CS, Scriven LE, Flickinger MC. 2007. Hydrogen production by photoreactive nanoporous latex coatings of nongrowing *Rhodopseudomonas palustris* CGA009. Biotechnol Prog 23:124–130. https://doi.org/10.1021/bp060254+
- 43. Guss AM, Rother M, Zhang JK, Kulkarni G, Metcalf WW. 2008. New methods for tightly regulated gene expression and highly efficient chromosomal integration of cloned genes for *Methanosarcina* species. Archaea 2:193–203. https://doi.org/10.1155/2008/534081
- van Kessel JC, Marinelli LJ, Hatfull GF. 2008. Recombineering mycobacteria and their phages. Nat Rev Microbiol 6:851–857. https://doi.org/10. 1038/nrmicro2014
- Huff J, Czyz A, Landick R, Niederweis M. 2010. Taking phage integration to the next level as a genetic tool for mycobacteria. Gene 468:8–19. https://doi.org/10.1016/j.gene.2010.07.012
- Huang H, Chai C, Yang S, Jiang W, Gu Y. 2019. Phage serine integrasemediated genome engineering for efficient expression of chemical biosynthetic pathway in gas-fermenting Clostridium Ijungdahlii. Metab Eng 52:293–302. https://doi.org/10.1016/j.ymben.2019.01.005
- Baltz RH. 2012. Streptomyces temperate bacteriophage integration systems for stable genetic engineering of actinomycetes (and other organisms). J Ind Microbiol Biotechnol 39:661–672. https://doi.org/10. 1007/s10295-011-1069-6
- Meereboer KW, Misra M, Mohanty AK. 2020. Review of recent advances in the biodegradability of polyhydroxyalkanoate (PHA) bioplastics and their composites. Green Chem 22:5519–5558. https://doi.org/10.1039/ D0GC01647K
- Sabbagh F, Muhamad II. 2017. Production of poly-hydroxyalkanoate as secondary metabolite with main focus on sustainable energy. Renew Sustain Energy Rev 72:95–104. https://doi.org/10.1016/j.rser.2016.11.012
- Karan H, Funk C, Grabert M, Oey M, Hankamer B. 2019. Green bioplastics as part of a circular bioeconomy. Trends Plant Sci 24:237–249. https://doi.org/10.1016/j.tplants.2018.11.010
- Bátori V, Åkesson D, Zamani A, Taherzadeh MJ, Sárvári Horváth I. 2018.
   Anaerobic degradation of bioplastics: a review. Waste Manag 80:406–413. https://doi.org/10.1016/j.wasman.2018.09.040
- Sirohi R, Prakash Pandey J, Kumar Gaur V, Gnansounou E, Sindhu R. 2020.
   Critical overview of biomass feedstocks as sustainable substrates for the production of polyhydroxybutyrate (PHB). Bioresour Technol 311:123536. https://doi.org/10.1016/j.biortech.2020.123536
- Brodin M, Vallejos M, Opedal MT, Area MC, Chinga-Carrasco G. 2017.
   Lignocellulosics as sustainable resources for production of bioplastics a review. J Clean Prod 162:646–664. https://doi.org/10.1016/j.jclepro. 2017.05.209
- Kourmentza C, Plácido J, Venetsaneas N, Burniol-Figols A, Varrone C, Gavala HN, Reis MAM. 2017. Recent advances and challenges towards sustainable polyhydroxyalkanoate (PHA) production. Bioengineering (Basel) 4:55. https://doi.org/10.3390/bioengineering4020055
- Maehara A, Doi Y, Nishiyama T, Takagi Y, Ueda S, Nakano H, Yamane T. 2001. PhaR, a protein of unknown function conserved among short-chain-length polyhydroxyalkanoic acids producing bacteria, is a DNA-binding protein and represses *Paracoccus denitrificans* phaP expression in vitro. FEMS Microbiol Lett 200:9–15. https://doi.org/10.1111/j.1574-6968.2001.tb10685.x

- York GM, Stubbe J, Sinskey AJ. 2002. The Ralstonia eutropha PhaR protein couples synthesis of the PhaP phasin to the presence of polyhydroxybutyrate in cells and promotes polyhydroxybutyrate production. J Bacteriol 184:59–66. https://doi.org/10.1128/JB.184.1.59-66.2002
- Červenka EJ. 2022. Optimizing PHB bioplastic accumulation in sinorhizobium meliloti grown on CO<sub>2</sub>-derived formate and bicarbonate. Queen's University (Canada).
- Koch M, Doello S, Gutekunst K, Forchhammer K. 2019. PHB is produced from glycogen turn-over during nitrogen starvation in *Synechocystis* sp. PCC 6803. JJMS 20:1942. https://doi.org/10.3390/ijms20081942
- Wang J, Yu H-Q. 2007. Biosynthesis of polyhydroxybutyrate (PHB) and extracellular polymeric substances (EPS) by *Ralstonia eutropha* ATCC 17699 in batch cultures. Appl Microbiol Biotechnol 75:871–878. https:// doi.org/10.1007/s00253-007-0870-7
- Li Z, Xin X, Xiong B, Zhao D, Zhang X, Bi C. 2020. Engineering the calvinbenson-bassham cycle and hydrogen utilization pathway of *Ralstonia* eutropha for improved autotrophic growth and polyhydroxybutyrate production. Microb Cell Fact 19:1–9. https://doi.org/10.1186/s12934-020-01494-y
- Higuchi-Takeuchi M, Morisaki K, Toyooka K, Numata K. 2016. Synthesis of high-molecular-weight polyhydroxyalkanoates by marine photosynthetic purple bacteria. PLoS One 11:e0160981. https://doi.org/10.1371/ journal.pone.0160981
- Kamravamanesh D, Pflügl S, Nischkauer W, Limbeck A, Lackner M, Herwig C. 2017. Photosynthetic poly-β-hydroxybutyrate accumulation in unicellular cyanobacterium *Synechocystis* sp. PCC 6714. AMB Express 7:143. https://doi.org/10.1186/s13568-017-0443-9
- Quandt J, Hynes MF. 1993. Versatile suicide vectors which allow direct selection for gene replacement in gram-negative bacteria. Gene 127:15– 21. https://doi.org/10.1016/0378-1119(93)90611-6
- Khan SR, Gaines J, Roop RM II, Farrand SK. 2008. Broad-host-range expression vectors with Tightly regulated promoters and their use to examine the influence of TraR and TraM expression on ti plasmid quorum sensing. Appl Environ Microbiol 74:5053–5062. https://doi.org/ 10.1128/AEM.01098-08
- Vacani PF, Malek MM, Davey PG. 1993. Cost of gentamicin assays carried out by microbiology laboratories. J Clin Pathol 46:890–895. https://doi. org/10.1136/jcp.46.10.890
- Phillips GJ. 1999. New cloning vectors with temperature-sensitive replication. Plasmid 41:78–81. https://doi.org/10.1006/plas.1998.1380
- Nishihata S, Kondo T, Tanaka K, Ishikawa S, Takenaka S, Kang C-M, Yoshida K-I. 2018. Bradyrhizobium diazoefficiens USDA110 PhaR functions for pleiotropic regulation of cellular processes besides PHB accumulation. BMC Microbiol 18:156. https://doi.org/10.1186/s12866-018-1317-2
- Kobayashi J, Kondo A. 2019. Disruption of poly (3-hydroxyalkanoate) depolymerase gene and overexpression of three poly (3-hydroxybutyrate) biosynthetic genes improve poly (3-hydroxybutyrate) production from nitrogen rich medium by *Rhodobacter sphaeroides*. Microb Cell Fact 18:40. https://doi.org/10.1186/s12934-019-1088-y
- Awogbemi O, Kallon DVV. 2022. Application of tubular reactor technologies for the acceleration of biodiesel production. Bioengineering (Basel) 9:347. https://doi.org/10.3390/bioengineering9080347
- Escapa IF, del Cerro C, García JL, Prieto MA. 2013. The role of GIPR repressor in *Pseudomonas putida* KT2440 growth and PHA production from glycerol. Environ Microbiol 15:93–110. https://doi.org/10.1111/j. 1462-2920.2012.02790.x
- Majerczak K, Wadkin Snaith D, Magueijo V, Mulheran P, Liggat J, Johnston K. 2022. Polyhydroxybutyrate: a review of experimental and simulation studies of the effect of fillers on crystallinity and mechanical properties. Polym Int 71:1398–1408. https://doi.org/10.1002/pi.6402
- Bjørnsen P, Riemann B. 1988. Towards a quantitative stage in the study of microbial processes in pelagic carbon flows. Ergebn Limnol 31:185– 193
- 73. Bratbak G, Dundas I. 1984. Bacterial dry matter content and biomass estimations. Appl Environ Microbiol 48:755–757. https://doi.org/10. 1128/aem.48.4.755-757.1984
- Arkin AP, Cottingham RW, Henry CS, Harris NL, Stevens RL, Maslov S, Dehal P, Ware D, Perez F, Canon S, et al. 2018. KBase: the United States department of energy systems biology knowledgebase. Nat Biotechnol 36:566–569. https://doi.org/10.1038/nbt.4163

- Wick R. 2024. Quality filtering tool for long reads. Available from: https://github.com/rrwick/Filtlong. Retrieved 11 Apr 2024.
- Andrews S. 2010. FastQC: a quality control tool for high throughput sequence data. Babraham Bioinformatics. Available from: http://www. bioinformatics. babraham. ac. uk/projects/fastqc
- Li H. 2016. Minimap and miniasm: fast mapping and de novo assembly for noisy long sequences. Bioinformatics 32:2103–2110. https://doi.org/ 10.1093/bioinformatics/btw152
- Kolmogorov M, Yuan J, Lin Y, Pevzner PA. 2019. Assembly of long, errorprone reads using repeat graphs. Nat Biotechnol 37:540–546. https://doi. org/10.1038/s41587-019-0072-8
- Gurevich A, Saveliev V, Vyahhi N, Tesler G. 2013. QUAST: quality assessment tool for genome assemblies. Bioinformatics 29:1072–1075. https://doi.org/10.1093/bioinformatics/btt086
- 80. Brettin T, Davis JJ, Disz T, Edwards RA, Gerdes S, Olsen GJ, Olson R, Overbeek R, Parrello B, Pusch GD, Shukla M, Thomason JA 3rd, Stevens R,

- Vonstein V, Wattam AR, Xia F. 2015. RASTtk: a modular and extensible implementation of the RAST algorithm for building custom annotation pipelines and annotating batches of genomes. Sci Rep 5:8365. https://doi.org/10.1038/srep08365
- Aziz RK, Bartels D, Best AA, DeJongh M, Disz T, Edwards RA, Formsma K, Gerdes S, Glass EM, Kubal M, et al. 2008. The RAST server: rapid annotations using subsystems technology. BMC Genomics 9:1–15. https://doi.org/10.1186/1471-2164-9-75
- Overbeek R, Begley T, Butler RM, Choudhuri JV, Chuang H-Y, Cohoon M, de Crécy-Lagard V, Diaz N, Disz T, Edwards R, et al. 2005. The subsystems approach to genome annotation and its use in the project to annotate 1000 genomes. Nucleic Acids Res 33:5691–5702. https://doi.org/10. 1093/nar/gki866
- Altschul SF, Gish W, Miller W, Myers EW, Lipman DJ. 1990. Basic local alignment search tool. J Mol Biol 215:403–410. https://doi.org/10.1016/ S0022-2836(05)80360-2